3 Two way influence of the atomic and electronic structure

3.1 Influence of the atomic on the electronic structure: The formation of Quantum Well States

In Chapter 1 it was described how the reduced dimensionality of metallic films leads to the formation of discrete energy states, commonly referred to as quantum well states (QWS). The formation of these states, and their behaviour as a function of thickness, partly depends on the nature of the overlayer material, and partly on that of the substrate. The overlayer material is important because the QWS are derived from the bulk band structure of the respective metal. In this chapter it will be shown that many properties of QWS, such as, for example, the number of states per monolayer and their behaviour as a function of photon energy, primarily depend on the nature of the overlayer material. Determining how the substrate influences the formation and character of QWS is more complex and will be a main issue throughout this thesis. In this chapter it will only be shown that the properties of different substrates can result in a widely varying behaviour of the QWS.
In order to be able to achieve a thorough comparison between overlayer materials and substrates, the formation and character of QWS in the following systems will be reported in this chapter. As examples of the strong influence of the substrate character on the QWS, Pb on Cu(111), Si(111)7x7, Si(111)√3 and graphitized SiC (hence graphite or C(111)) will be used. To compare different overlayer materials, indium on Si(111)7x7 and Si(100), and aluminium on graphite are included. Aluminium films on silicon have already been extensively studied[1] and these results are used here for comparison.

3.1.1 Quantum Well States in thin Pb films

In order to obtain a better understanding of the experimental results for quantum well states in Pb overlayers, it is helpful to predict their energies and bandshape, by only considering the Pb bulk band structure and interlayer spacing. For Pb, the interlayer spacing along the (111) direction, d_0 is 2.86 Å, and the Fermi wavevector λ_F is 3.95 Å, hence the ratio of these quantities is $2d_0 \approx 3\,{}^{\lambda_F}/_{2}$. This means that, for every two monolayers of Pb, three extra nodes of the quantum well envelope function will fit in. This deduction is valid for the entire occupied s-p valence band. The lower band (between 8 and 12 eV binding energy in Figure 3.1) will, however, accommodate a new QWS for every additional atomic layer since it extends over the entire Brillouin zone. In the upper valence

1 L. Aballe, PhD Thesis, Freie Universität Berlin (2001).

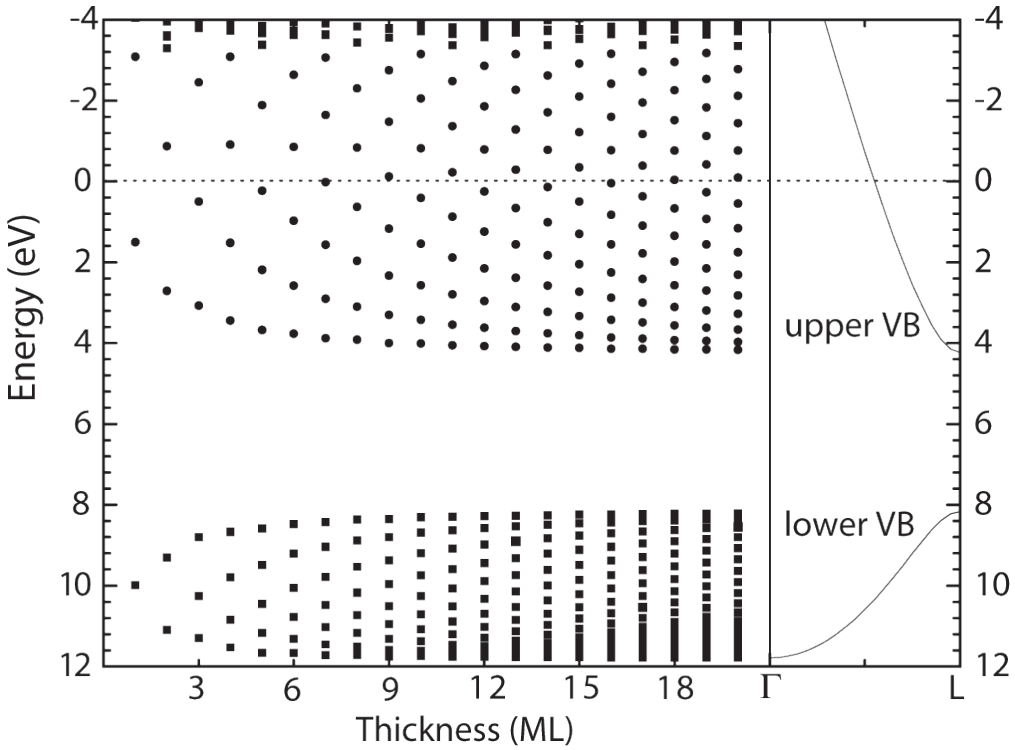

Figure 3.1: Calculated quantum well state binding energies as a function of coverage for free-standing Pb slabs. The values have been obtained by M.Y. Chou from DFT calculation[2]. On the right hand side the bulk band structure from which the QWS are derived, is displayed.

band (between 4 eV and the Fermi level), which is the main object of this study, a new QWS can therefore be expected to drop below the Fermi level for every second monolayer. This results in the same observation as "cutting up the bulk band structure". Because the upper s-p band passes through the Fermi level approximately halfway through the Brillouin zone, an new QWS will appear with the deposition of every second layer. First principle DFT calculations for free-standing Pb slabs[2] show such a development of QWS binding energy as a function of coverage, as shown in Figure 3.1. The quantum well state energies obtained from these calculations, combined with the development of QWS with coverage, can be used to obtain the exact coverage and deposition rate.

Valence band spectra of Pb films deposited at low temperature on the clean Cu(111) substrate are displayed in Figure 3.2[3], with the total coverage indicated on the right hand side of each spectrum. Individual peaks that shift with coverage can be observed, indicating that they depend on the thickness of the Pb layer, and are thus caused by quantization phenomena. Using the phase accumulation model presented in Chapter 1, and the DFT calculations from Figure 3.1, the exact thickness of the layer that the individual quantum well states originate from can be identified; these are indicated next to the respective states. Taking the spectrum obtained for 7.2 ML of Pb as an example, peaks can be observed at 0.2 and 0.7 eV binding energy. Trying to assign these two peaks

2 C.M. Wei and M.Y. Chou, Phys. Rev. B **66**, 233408 (2002).

3 J.H. Dil, J.W. Kim, S. Gokhale, M. Tallarida, and K. Horn, Phys. Rev. B **70**, 045405 (2004).

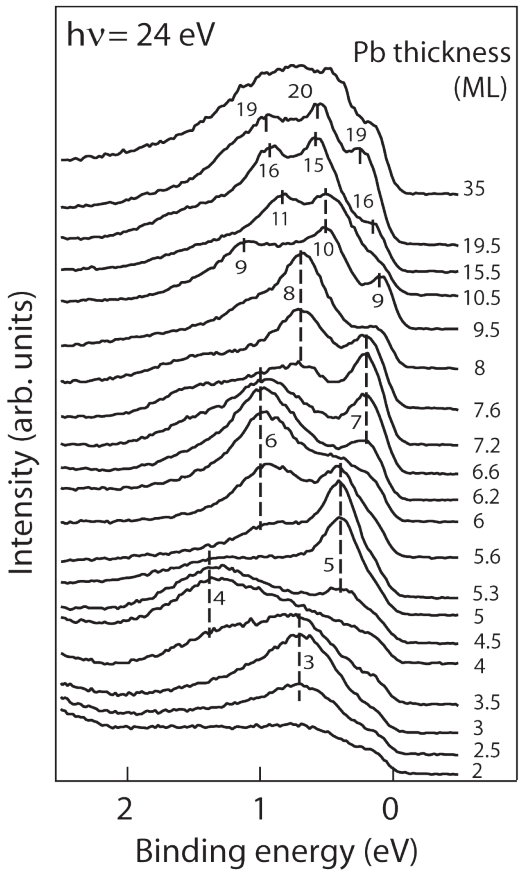

Figure 3.2: Valence level photoemission spectra from Pb layers on Cu(111) deposited at 100 K, for different total depositions as indicated on the right. The numbers next to the peaks indicate the layer thickness that the QWS originate from. The spectra are recorded at normal emission at a photon energy of 24 eV[3].

to one single coverage, would, on basis of the energy spacing between the QWS, require a layer of more than 20 ML thickness. This suggests that either the Pb film organizes in 20 ML high islands, which is unlikely and was not observed in STM[4], or that several films of different thicknesses contribute to the spectrum. After all, the spectrum is an incoherent superposition of a large (~1 mm diameter) region of the sample, and thus a signal from different layers could be present. Using only the energy positions of the QWS and not taking the total coverage into account, only single spectra, and not the entire deposition series as shown in Figure 3.2 can be fitted. It is therefore clear that this is not the correct approach. For a 7 ML thick film, on the other hand, the energy spacing would be around 1.5 eV. This leads to the conclusion that the peaks originate from different coverages, and these are, according to the phase accumulation model, 7 and 8 ML thick, respectively.

From the development of QWS with coverage as indicated in Figure 3.2, it can be observed that a layer starts to grow only when the previous layer is completed. The growth mode can therefore be characterized as layer-by-layer growth. This corresponds to observations in He scattering experiments for this system by Braun and Toennies[5], and contradicts the concept of bilayer growth suggested by Hinch *et al*.[6], since in the spectra features from consecutive odd and even layers are present, but never from a mixture of N and N + 2 monolayers.

4 R. Otero, A.L. Vazques de Parga, and R. Miranda, Phys. Rev. B **66**, 115401 (2002).

5 J. Braun and J.P. Toennies, Surf. Sci. **384**, L858 (1997).

6 B.J. Hinch, C. Kozoil, J.P. Toennies, and G. Zhang, Europhys. Lett. **10**, 341 (1989).

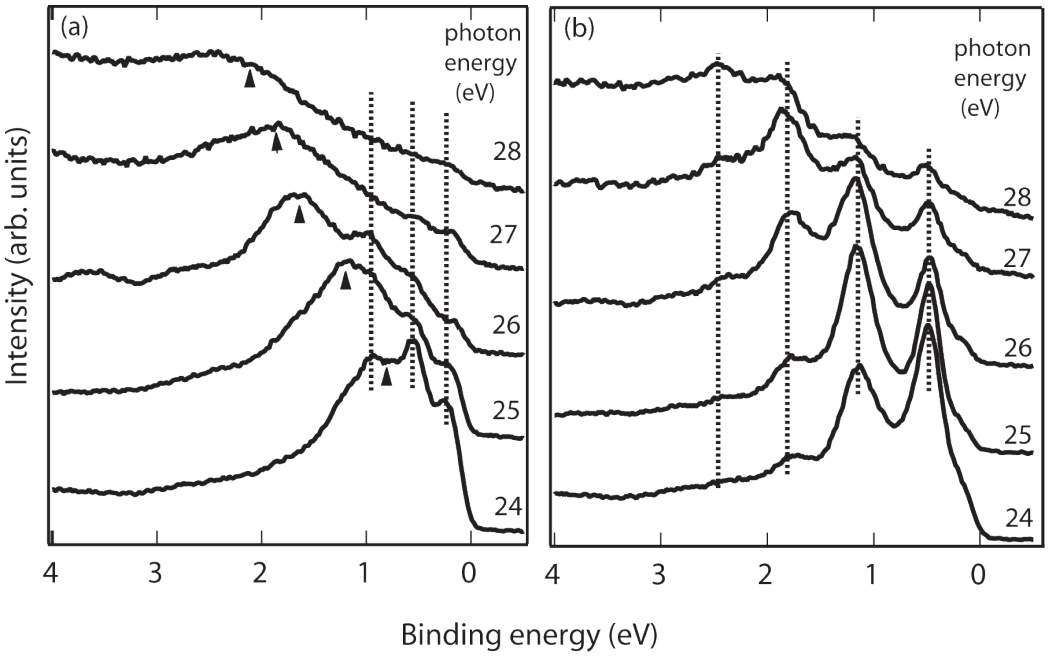

Figure 3.3: (a) Set of spectra from an unannealed 19.5 ML Pb film on Cu(111), recorded in normal emission as a function of photon energy as indicated near the spectra. Dotted lines indicate observed peaks due to quantum well states, the arrows indicate the band dispersion for bulk Pb. (b) Same set of data after annealing the layer to room temperature. Note the increased peak-to-valley ratio, and the energy shift and number of QWS. Figure from Ref. 3.

Annealing of Pb layers induces remarkable changes in the photoelectron spectra, as shown from a comparison of spectra from as-deposited and annealed films for different photon energies in Figure 3.3, for a thickness of 19.5 ML. A broad peak ranging from E_F up to 1.5 eV binding energy (E_B) occurs for the as-deposited film (Figure 3.3(a)), with several smaller, quantum-well derived peaks superimposed. This feature develops, upon annealing, into a set of sharp and well-defined peaks, with a large peak-to-valley ratio, reaching up to about 3 eV binding energy. The effect of annealing (Figure 3.3(b)), can be directly seen from the separation of quantum well peaks indicated by dotted lines. The spacing of 0.66 eV is characteristic for a 22 ML thick quantum well. This comparison is made for several photon energies, centred at $h\nu = 26$ eV. The first observation is that the features identified as quantum well states do not shift with photon energy (and thus with the normal component of the wave vector), confirming again the confinement in the surface normal direction, i.e. k_z is no longer a good quantum number. The broad peak in the unannealed film, however, on which the quantum well peaks are superimposed, does move with photon energy, and so does the envelope of the sharp peaks in the spectrum from the annealed surface. By comparison with the direct bulk band transition[7] indicated by the triangles, it is clear that the broad feature in Figure 3.3(a) has a strong bulk character, and that the modulation of intensities in Figure 3.3(b) is likewise induced by a bulk transition.

The mechanism behind the observation that the intensity of QWS is modulated by the bulk transition, although the states are confined in the direction normal to the surface, is because the

7 K.Horn, B. Reihl, A. Zartner, D.E. Eastman, K. Hermann, and J. Noffke, Phys. Rev. B **30**, 1711 (1984).

states originate from a quantization of the bulk band. The first to use QWS to map the unoccupied band structure was Neuhold[8], and also Mugarza *et al*. have used such intensity modulations to map the unoccupied band structure of Cu(100) by studying thin Cu films on Co(100)[9].

The comparison between as-deposited and annealed layers in Figure 3.3 is made for a relatively thick layer, namely 19.5 ML. That the strong change in the valence band spectra upon annealing is not limited to thicker films is indicated in Figure 3.4. Here electron distribution curves are shown for coverages ranging from 2.5 to 19.5 ML, before (dashed lines) and after anneal (solid lines). For all coverages, the quantum well states become more pronounced after annealing the layer, and the changes are not limited to coverages where there is a mixture of layers present. For the 17 ML thick film, for example, a new peak now arises that was not present before annealing. In Section 3.2, concerned with the influence of the electronic structure on the atomic structure of the layers, the mechanism responsible for the changes observed in Figure 3.4 will be discussed.

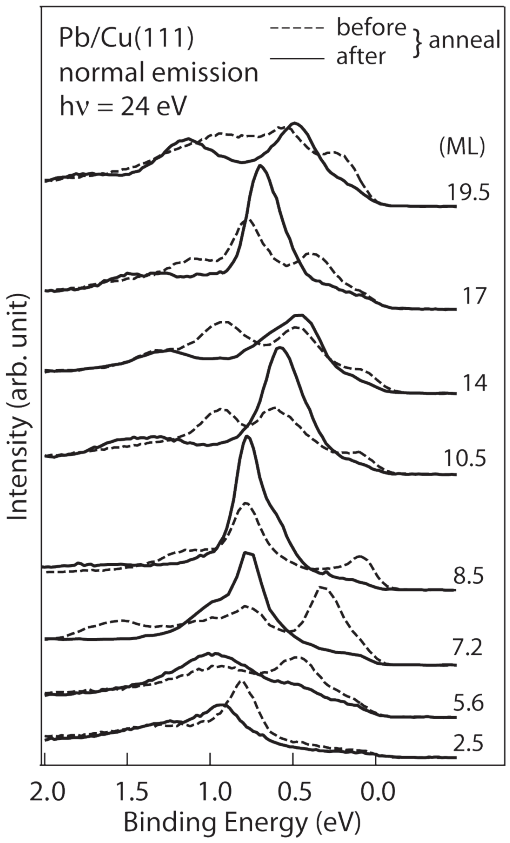

Figure 3.4: Close-up of spectra near E_F of as-deposited Pb films on Cu(111) (dashed lines) of different thickness, and the changes induced by annealing (solid lines). The data is recorded at normal emission with a photon energy of 24 eV. From Ref. 3.

Pb on Si(111)7x7 follows a growth mode that is different from that observed on Cu(111). In Figure 3.2, the QWS can be seen to abruptly change with increasing coverage, the situation is quite different for Pb/Si(111)7x7, as shown in Figure 3.5. Here the features disperse smoothly with increasing coverage, comparable to previously observations for the same system[10]. An interpretation in terms

8 G. Neuold, PhD Thesis, Freie Universität Berlin (1996).

9 A. Mugarza, J.E. Ortega, A. Mascaraque, E.G. Michel, K.N. Altmann and F.J. Himpsel, Surf. Sci. **482-485**, 464 (2001).

10 A. Mans, J.H. Dil, A. Ettema, and H.H. Weitering, Phys. Rev. B **66**, 195410 (2002).

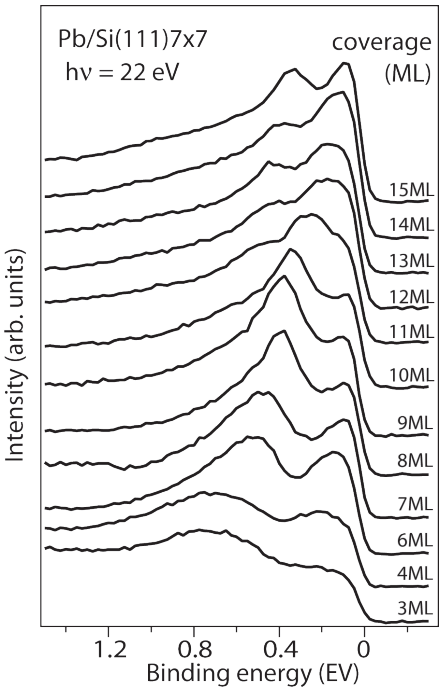

Figure 3.5: Valence band spectra for Pb layers on Si(111)7x7 deposited at 100 K for different coverages as indicated on the right. The spectra are obtained at normal emission at a photon energy of 22 eV.

of the growth mode can be given from these data by comparison to calculations. Figure 3.6 shows two different sets of simulated photoemission spectra. The spectra were modelled by applying a Gaussian energy broadening of 0.15 eV to the quantum well energy positions resulting from DFT calculations[2]; this broadening is comparable to the full width at half maximum (FWHM) of the peaks observed in the experimental spectra. Besides the spectral broadening in the energy direction, also a Gaussian broadening in the coverage direction has been added. This resembles the situation where the layer height distribution on the entire surface that is probed, has the same Gaussian distribution. In Figure 3.6(a) the broadening has been set to 1 ML, which means that the development of QWS should resemble that of layer-by-layer growth. The correspondence with Figure 3.2 is significant, confirming again the assumption that for Pb/Cu(111) layer-by-layer growth is the relevant mechanism. Figure 3.6(b) shows simulated spectra with the same energy broadening, but with a Gaussian coverage broadening of 1.4 ML. This represents a rough growth front, where for a coverage of N monolayers, parts of the surface will consist of N - 1, N, and N + 1 layers. The spectral features presented in this image, model the overall development of the QWS in Figure 3.5. Co-existence of consecutive even (or odd) coverages, effectively leads to a substantial broadening of the lines, and conclusions for seperate layers cannot be drawn based on this data.

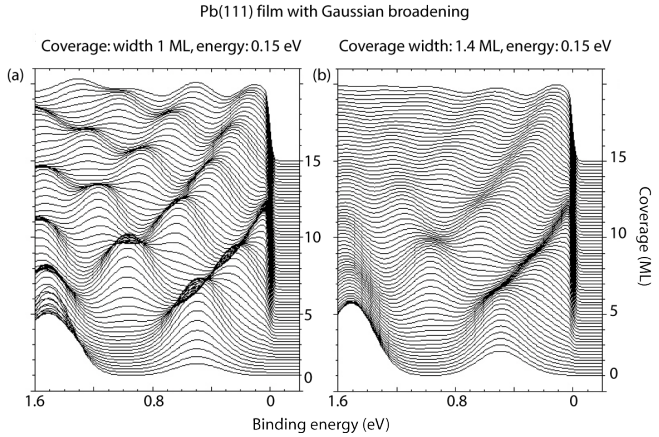

Figure 3.6: Simulated spectra for Pb based on the QWS binding energies obtained from DFT. The spectra have been artificially broadened in the energy direction with 0.15 eV, and in the coverage direction with 1 ML (a) and 1.4 ML (b) .

That the rather broad features in Figure 3.5 are actually QWS is obvious from Figure 3.7(a). Here the valence band spectra for a 12 ML thick as-deposited film are shown for a variety of photon energies. Although the bulk-like feature again disperses with photon energy, there are some weaker lines that remain at the same position for all excitation energies; these lines are therefore definitely derived from states which are confined in the direction normal to the surface. An analysis of the energy positions of the QWS reveals that they originate from a mixture of 11, 12, and 13 ML thick layers. After a mild anneal, the spectra change dramatically (Figure 3.7(b)). An extremely sharp QWS develops at 0.48 eV that can be followed up to 30 eV photon energy. The dispersing bulk feature has disappeared, and only the relative intensities of the QWS change as a function of photon energy. As can be concluded from a comparison of Figures 3.3 and 3.7, the changes induced by annealing are similar for Pb on Cu(111) and on Si(111)7x7. There is, however, one major difference: the Pb quantum well states on Cu(111) all are approximately equally sharp, regardless of their binding energy. On Si(111)7x7, on the other hand, the QWS at 0.48 eV is much sharper than the state at 1.38 eV binding energy. The different behaviour of both systems is most likely due to the differences in lattice mismatch between Pb/Si and Pb/Cu, which are 9 % and 30 % respectively. The proximity of the bulk band edge of Si alone cannot explain the change in QWS width, because for Cu(111) there is also a band edge in the same energy range. How these properties of the interface can account for the difference in valence band spectra will be discussed in Chapter 4.

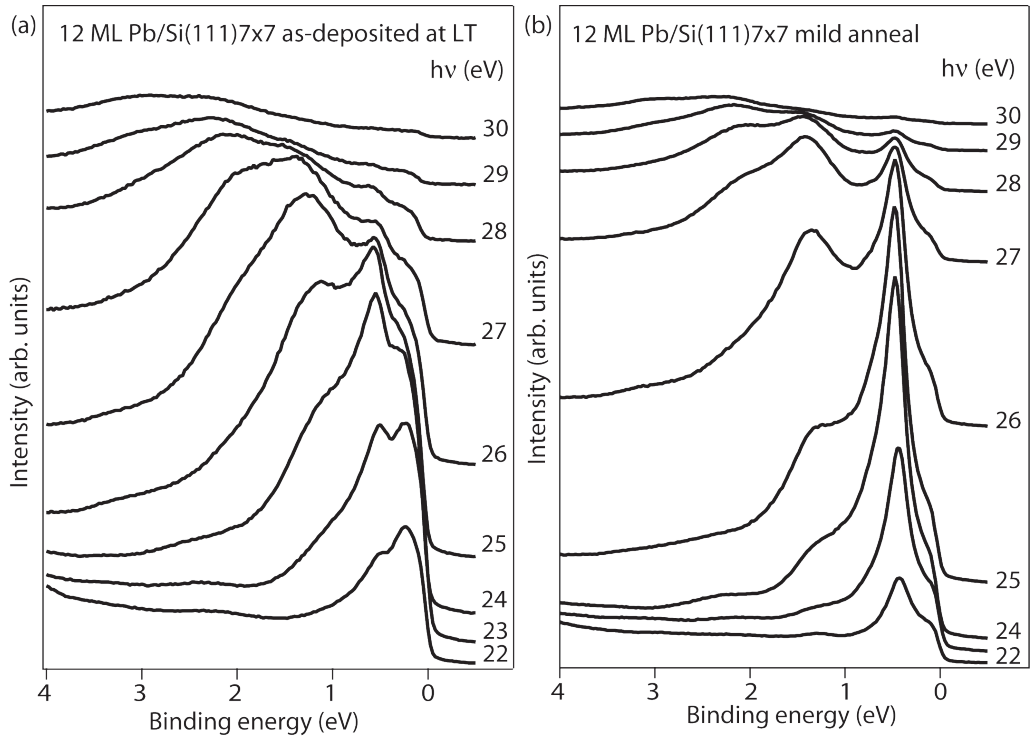

Figure 3.7: (a) Set of spectra from an unannealed 12 ML Pb film on Si(111)7x7 deposited at 100 K, recorded in normal emission as a function of photon energy as indicated at the spectra. (b) Same set of data after giving the layer a mild anneal.

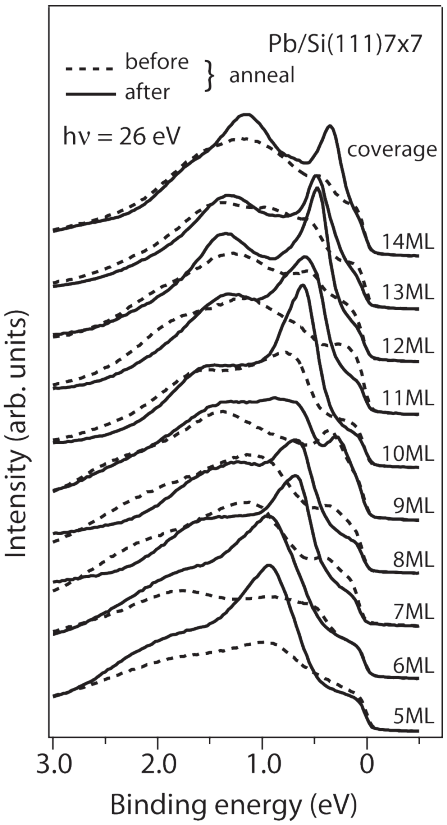

Figure 3.8: Valence level spectra of as-deposited Pb films on Si(111) (dashed lines) of different thickness, and the changes induced by annealing (solid lines). The data is recorded at normal emission with a photon energy of 26 eV.

From the absolute position of the QWS in Figure 3.7(b) and their spacing, I conclude that after annealing the layer the influence of the rough growth front is reduced, and that only a 13 ML thick film remains. Similar changes also occur for other coverages, as can be seen in Figure 3.8. Here, spectra are shown for different coverages, where the dashed lines represent the as-deposited and the solid lines the annealed layers. The data was recorded with a photon energy of 26 eV, where the as-deposited layers exhibit a rather featureless valence band spectrum with intensity primarily from the broad bulk-like transition. After annealing, for all coverages well defined QWS are formed, the binding energy position of which is seen to change with increasing coverage. Apart from a very sharp state within a region of approximately 1 eV below the Fermi level, for all coverages a second, less sharp feature is observed. The position of this second line changes with coverage, indicating that it is also a state derived from confinement of the electrons in the direction perpendicular to the surface. These two states are thus QWS that belong to a single layer height, indicating the reduction of the previously mentioned rough growth front.

For the previous two systems, (Pb/Cu(111) and Pb/Si(111)7x7), annealing of the overlayer was necessary to obtain sharp QWS that could be assigned to a single coverage. This is not necessary for Pb deposited at 100 K on the $\sqrt{3}$x$\sqrt{3}$ reconstructed Si(111):Pb surface. Figure 3.9 shows energy distribution curves for a 10 ML thick film deposited on the Si(111)$\sqrt{3}$ substrate, recorded with photon energies of 24 and 28 eV. The peak to valley ratio is comparable to the results for the Pb films on Si(111)7x7 after anneal, with a very intense and sharp QWS in the region within 0.8 eV below the Fermi level. Besides this QWS and the broad, but not very intense, bulk-like transition that shifts with photon energy (Figure 2.14), no other states are observed. The development of the QWS with coverage is displayed in Figure 3.10. Instead of energy distribution curves, here the complete binding energy vs.

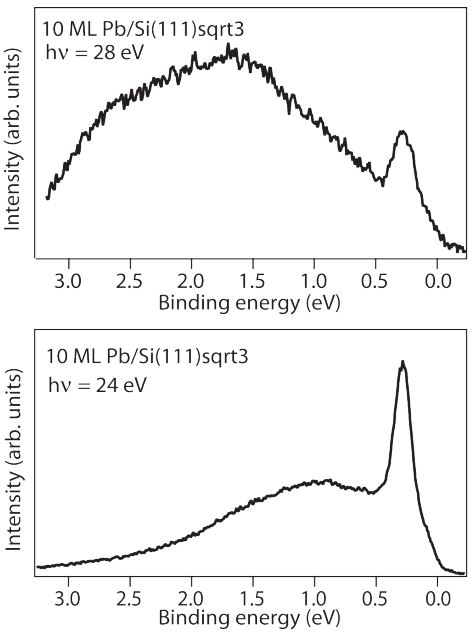

Figure 3.9: Spectra of a 10 ML thick Pb layer on Si(111)$\sqrt{3}$, recorded at normal emission for a photon energy of 28 eV (top) and 24 eV (bottom).

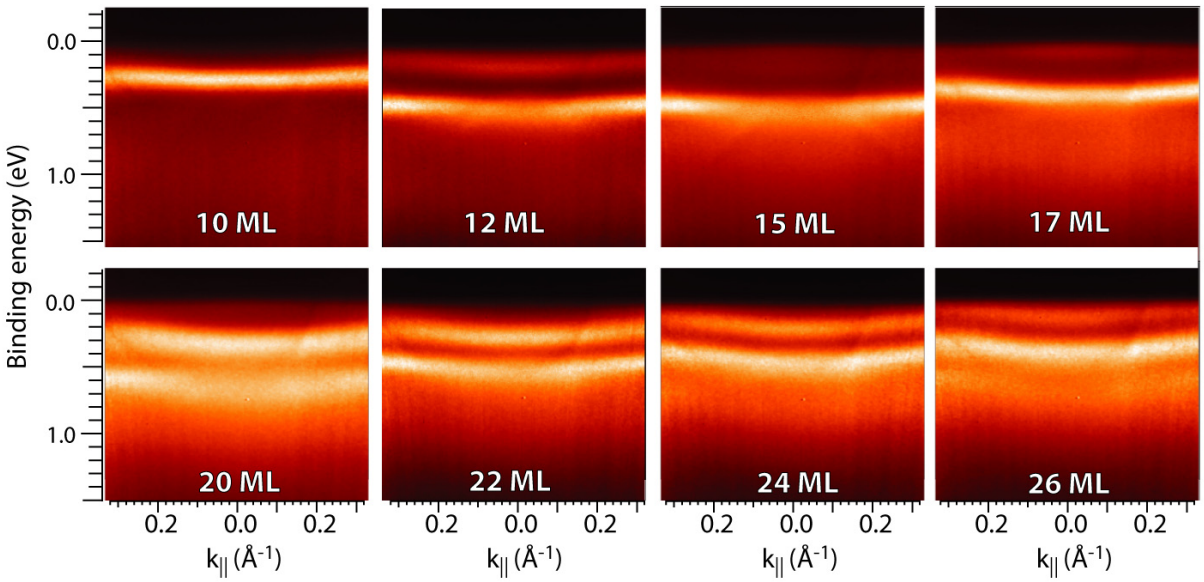

Figure 3.10: Energy vs. $k_{||}$ photoemission images for different Pb coverages on Si(111)√3x√3, measured around normal emission with a photon energy of 24 eV. Lighter colours indicate higher electron density. Small intensity modulations, in for example the 15 ML image, are due to interaction with the substrate bands as described in Section 4.4. The shape of the QWS presented here, i.e. the small dispersion with $k_{||}$, is discussed in Section 5.1.

k-parallel images (obtained with the Phoibos 100 analyser as described in Chapter 2) are shown for different coverages. The EDC in Figure 3.9 for a photon energy of 24 eV has actually been extracted from the respective image by plotting the intensity at $k_{||} = 0$ for the 10 ML thick film as a function of binding energy. In the images, the absence of states outside the 1 eV window below the Fermi level is striking. The fact that for the 26 ML thick film, two well separated QWS can be observed, which both belong to the same coverage, indicates the good crystalline quality of the layers. Note also some minor intensity variations in the QWS peaks. These are due to an interaction between the substrate bulk states and the QWS[11,12] as discussed in Section 4.4.

The development of the QWS peaks with coverage agrees very well with the theoretical predictions. From Figure 3.1 it is expected that a new quantum well state appears at approximately the same energy position upon increasing the film thickness by three monolayers. This is actually observed for the 12 and 15 ML thick film. Here, due to intensity normalization in the images, the lower binding energy state for the 15 ML film is only weakly apparent. Moreover, one would expect that the QWS of consecutive even or odd layers lie close to each other, and would appear to shift slightly downwards in binding energy. Considering the 20 to 26 ML deposition series, this is exactly what is experimentally observed: the two visible QWS slightly move towards the Fermi level come closer. In the 26 ML film, a third QWS becomes apparent at the higher binding energy side, and it appears that for higher coverages the uppermost QWS will move through the Fermi level. This apparent movement towards lower binding energies is caused by a visual artefact. With

11 L. Aballe et al. Phys. Rev. Lett. **87**, 156801 (2001).

12 S.-J. Tang, L. Basile, T. Miller, and T.-C. Chiang, Phys. Rev. Lett. **93**, 216804 (2004).

increasing coverage, and thus width of the potential well, the energy levels move down towards lower absolute energies. The next QWS that becomes occupied is, however, only at a slightly lower binding energy and the states appear to move upward. The state with quantum number n will shift about 0.5 eV away from the Fermi level for a 2 ML increase in the studied coverage regime, whereas the state with quantum number $n + 3$ for the 2 ML thicker film, will appear around 0.1 eV closer to E_F. Using the reduced quantum number p, defined as $p \equiv 3N - 2n$ in reference 10, the observed motion of the QWS towards the Fermi level can directly be understood. This quantum number gives an indication of the apparent motion of the QWS as a function of coverage. The state from N ML with quantum number n has the same value for p as the state from $N + 2$ ML with quantum number $n + 3$. From these considerations, I conclude that the Pb films grow in a perfect layer-by-layer manner, and the high intensity and large peak-to-valley ratio of the QWS is a signature of the very good crystalline quality of the layers.

In Chapter 2 the graphitized SiC surface was introduced as an ideal substrate to study the properties of overlayer materials with a minimum of substrate influence. Judging from photoemission results shown in Figure 3.11, Pb layers grown on this single crystal hexagonal graphite surface, are structurally at least equally well organized as those obtained on Si(111)√3. Several $k_{||}$ versus energy images, recorder at different polar angles with the Phoibos 100 CCD, can be combined to obtain a line cut through the surface Brillouin zone (SBZ) as displayed in Figure 3.11. This image is obtained from a total coverage of 2 ML of Pb on graphite. It covers $k_{||}$-space from the boundary of the Brillouin zone at $\overline{M}$ through the zone centre $\overline{\Gamma}$ into the centre of the next Brillouin zone, $\overline{\Gamma}'$, i.e. a data range of 85° polar angle in electron emission. The fact that well defined features can be detected over such a wide angular range is an indication for the good crystalline quality of the islands, because electrons have a long path in the film without losing their phase information. The

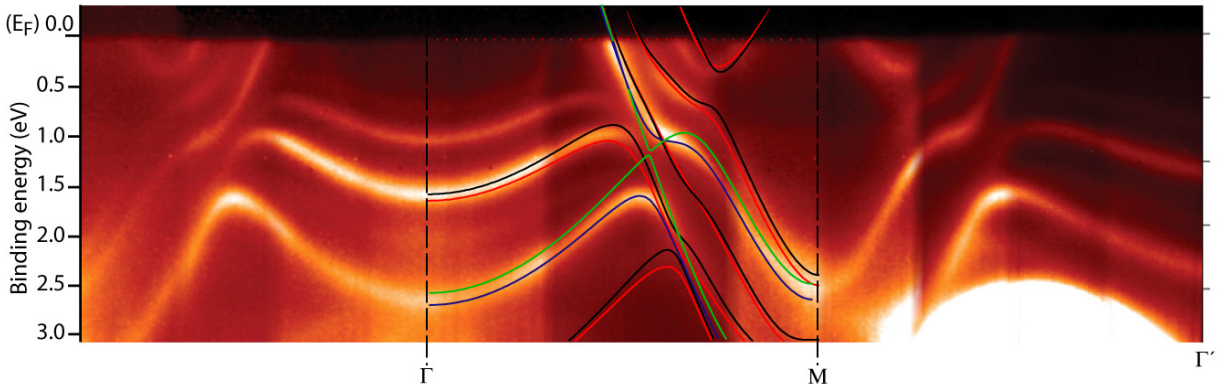

Figure 3.11 (colour): Cut through the surface Brillouin zone along the Γ-M direction for Pb on single crystalline graphite, obtained at a photon energy of 24 eV. The full image consists of several energy vs. angle photoemission images placed next to each other, hence the variations is background intensity. Superimposed on the images is the band structure obtained from DFT calculations including and excluding spin-orbit-coupling. For 4 ML the black line is without SOC, the red line with SOC, for 2 ML the green line is without SOC and the blue line with SOC. For a further description of the image see text.

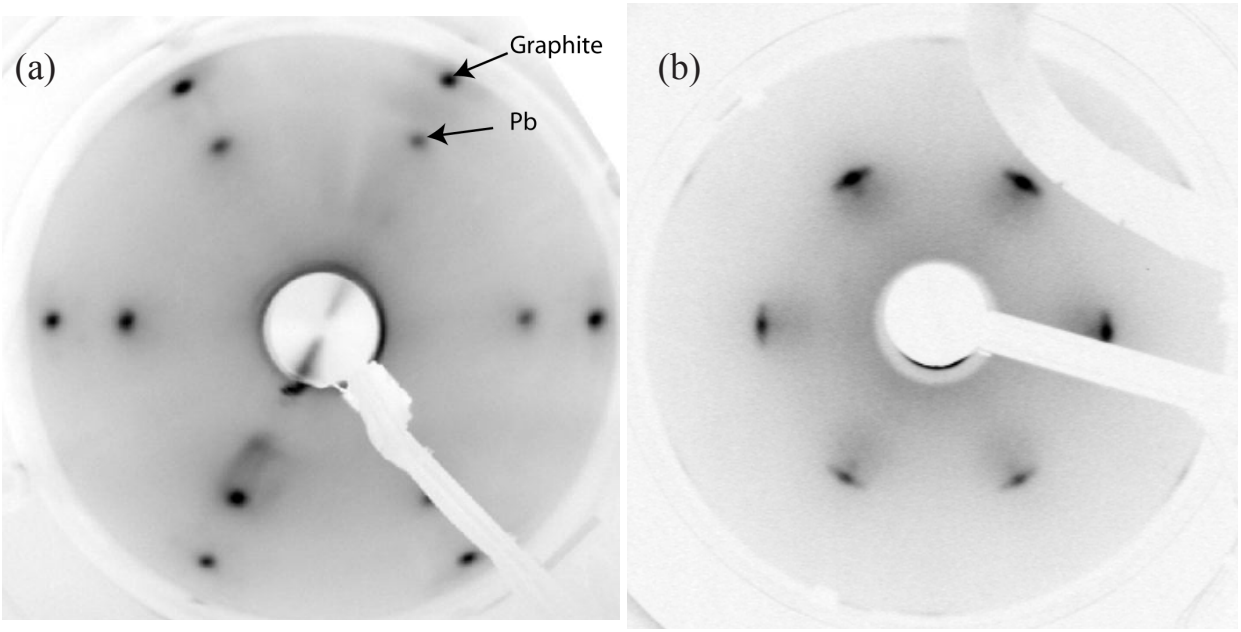

Figure 3.12: LEED patterns from (a) Pb on single crystalline hexagonal graphite obtained with an electron energy of 90 eV, and (b) an 8 ML thick layer of Pb on Si(111)7x7 at 87 eV. Note the large difference in rotational spread of the diffraction spots.

good crystalline quality of the film is confirmed by the sharp LEED spots in Figure 3.12(a). The inner spots originate from the Pb islands, and the outer spots from the graphite substrate, giving a graphic representation of the large lattice mismatch between the two materials. For comparison, a LEED image of Pb on Si(111)7x7 is shown in Figure 3.12(b). Here the large angular spread of the Pb spots can be directly observed, which is an indication of rotational disorder in the films. The absence of this spread in the LEED pattern from the Pb layers on graphite again indicates that the crystalline quality of these layers is much better.

Apart from the QWS (which will be discussed in more detail below), Figure 3.11 shows a variety of other features. The most profound of these is the region of high intensity between $\overline{M}$ and $\overline{\Gamma}'$ below a binding energy of 2.5 eV. This state originates from the C(111) substrate and is deliberately overexposed in order to be able to view the QWS features in this $k_{||}$ region. The fact that this state is the only substrate feature in the full energy and $k_{||}$ range of the image, confirms the unique suitability of graphite in order to study QWS without an influence from the substrate. Throughout the image, several vertical lines or more precisely intensity variations, can be observed. These are technical artefacts caused by the fact that the full image is composed of 12 individual images with an angular separation of 7°. Each of these images has its own optimal contrast and intensity, partly due to the change in the transition elements with changing exit angle, and partly due to the presence of other states. For all the images presented throughout this thesis optimal display parameters were carefully evaluated, in order to avoid altering the information in the picture just to obtain better quality images. The necessity to carefully consider the displaying parameters, is a problem that is typical for the use of images in data presentation and is not encountered when spectra are shown.

At the zone centre in Figure 3.11, strong emission from three quantum well states can be readily identified, at 1.07 eV, 1.63 eV, and 2.75 eV binding energy; weaker features are visible at 0.65 and 2.1 eV. Taking the energy spacing between the QWS and their relative intensities into account in the manner described above, it is obvious that the states belong to islands of different height. A similar conclusion can be drawn from the fact that, for relatively high total coverages of Pb, the graphite spots are still clearly visible in the LEED pattern, indicating that large areas of the bare surface exist between islands. A direct comparison of the measured quantum well state binding energies to the first-principle density functional theory calculations from Figure 3.1, in order to deduct the height of the individual islands, is not straightforward based solely on these energy values for one deposition. As mentioned before, many QWS originating from different layer heights may have the same binding energy. The QWS at 1.63 eV, for example, occurs at almost exactly the same binding energy for every increment of 3 monolayers. This state can therefore belong to either 1, 4, 7, or 10 ML, and the presence of other states is an indication of the exact island height. For 10 ML high islands, a second similarly intense state is expected at around 0.4 eV binding energy. This state is, however, not observed in Figure 3.11, and certainly not with a similar intensity as the state at 1.63 eV.

Assigning the different QWS to their respective island height hence is only possible in photoemission by studying the development of the states with increasing coverage. Figure 3.13 shows a series of electron distribution curves, obtained by plotting the intensity at $k_{\parallel} = 0$ as a function of binding energy. The total coverage is increased by steps of 1 ML (except between the second and third

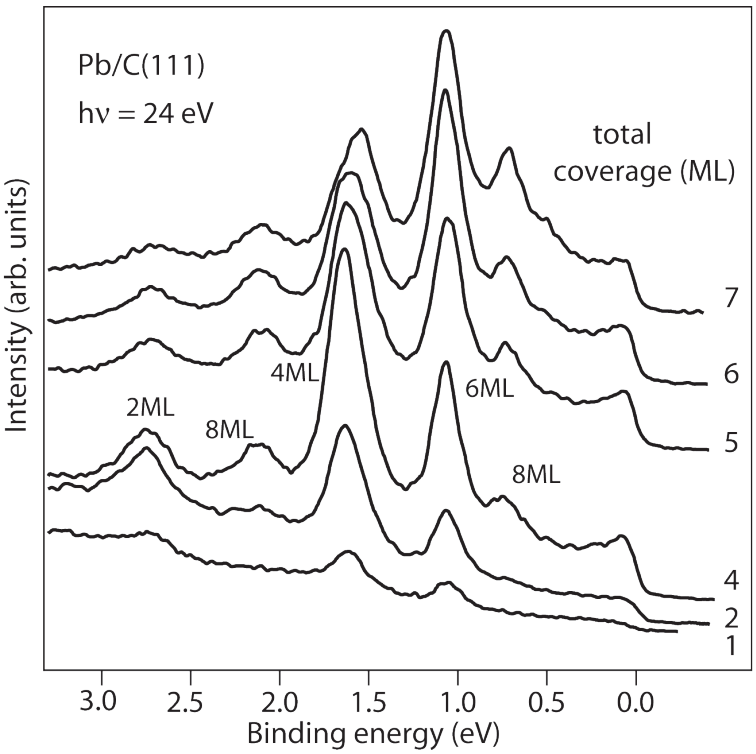

Figure 3.13: Valence level spectra of Pb on graphite at normal emission for different total coverages at 100 K, obtained with a photon energy of 24 eV. Next to the peaks the island heights of which the QWS are derived are indicated.

deposition where the increase is 2 ML) between measurements. The features present after the second deposition (corresponding to Figure 3.11), remain stationary for all higher coverages; changes occur only in the relative intensity of the quantum well states. Note that for the clean substrate (not shown in the plot) there are no features in the energy area studied[13]. For increasing coverages, it can be assumed that features belonging to thicker island will increase, and those originating from thinner islands will slowly decrease. Also, QWS belonging to the same island height should increase/decrease in in intensity in a similar fashion. Taking these considerations into account, and using the binding energies obtained from calculations for free-standing Pb layers as a reference, the QWS can be assigned as indicated in Figure 3.13. The state with the lowest binding energy belongs to the 8 ML thick islands, the next peak to 6 ML, then 4 ML and the other QWS from 8 ML, and the highest binding energy peak belongs to both 2 ML and 6 ML thick islands. Deviations from the calculations are less than 50 meV for all QWS, indicating that the layers experience no influence from the substrate and are thus quasi free-standing. This system therefore poses the nearest example to a free-standing film so popular in calculations, and can be used as a cross-check for these calculations; I am not aware of a similarily useful substrate for such puposes.

That the calculations performed for free-standing Pb layers are not only capable of predicting the binding energy of the QWS at the zone centre, but also reproduce the in-plane dispersion of the QWS throughout the entire SBZ, can be confirmed from the inset of the calculated band structure in Figure 3.11. Here the QWS band structure for a 2 ML and a 4 ML thick free-standing Pb slab is shown in one half of the surface Brillouin zone. Figure 3.14 also shows the DFT results for a 2 ML slab. Here both the occupied and unoccupied states are shown in order to obtain a better picture of the origin of the states from. As an additional test, calculations have been performed both incorporating and ignoring spin-orbit-coupling (SOC). For a high-Z material such as lead, it is expected that SOC has an influence on the band structure; this is exactly what can be observed in the calculations. The bands where the spin-orbit-coupling is taken into account fit best to the measured data in Figure 3.11. Especially around the avoided crossings, the influence of SOC seems to be strong, the QWS energies at the zone centre are, however, not influenced. In the calculated data presented in Figure 3.14, it is possible to identify the symmetry or orbital character of the individual bands. The lines that show a upward dispersion around the zone centre are derived from the $6p_z$ states; those high above the Fermi level at the Γ point and dispersing downward to cross the Fermi level around halfway through the SBZ, are derived from the $6p_x$ and $6p_y$ states. The reason for this distinction and the shape of the band, is schematically depicted in the inset in Figure 3.14. The p_z states are most bonding at $k = 0$, resulting in the lower energy, and most antibonding at the zone boundary, whereas for the $p_{x,y}$ states the opposite is true. Avoided crossing between these states and the $6p_z$ bands can be easily identified, resulting in the characteristic s-shape of the $6p_{x,y}$ bands. The details of the measured band structure in Figure 3.11 are reproduced in the DFT

13 T. Seyller et al. Surf. Sci. in press.

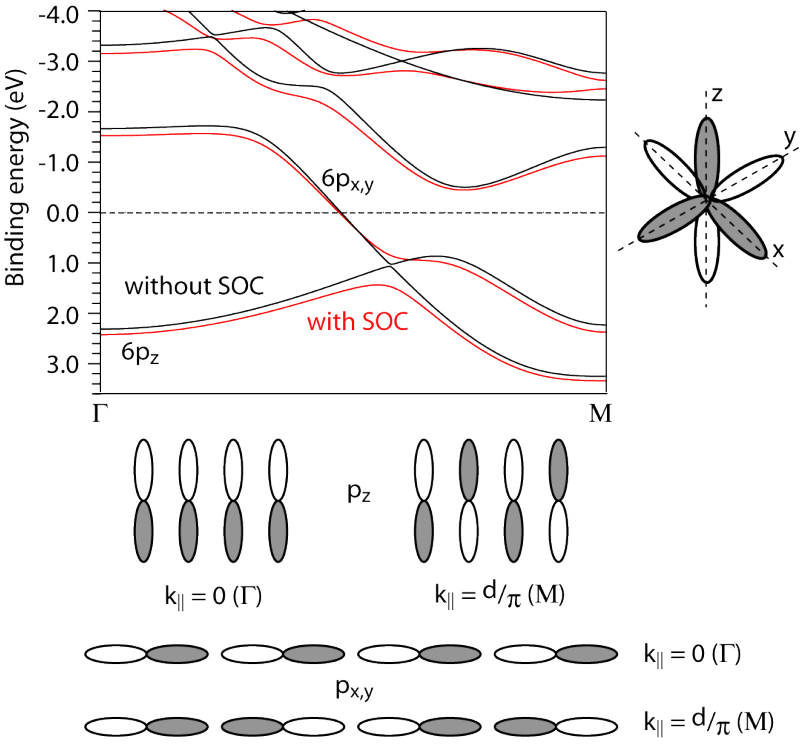

Figure 3.14: (top) Band structure of a 2 ML thick free standing Pb film from DFT calculations. The lighter colour lines represent the bands with spin-orbit coupling incorporated in the calculations, the dark lines those without spin-orbit coupling. (right) Simplified picture of the outer p-orbitals. (bottom) Explanation based on the bonding (lower energy) and anti-bonding (higher energy) of the p-orbitals, of why the p_z derived QWS exhibit an upward dispersion around Γ, and the $p_{x,y}$ derived bands disperse down. Calculations from B. Hülsen.

calculations incorporating SOC, especially the exact shape of the $6p_{x,y}$ bands is reproduced well. For the Pb derived QWS, the $\overline{\Gamma}$ and $\overline{M}$ points provide the expected mirror symmetry lines in the total bandstructure.

Briefly summarizing these results, Pb films deposited on Si(111), Cu(111) or graphite, form atomically smooth layers. On the Cu(111) and Si(111)7x7 substrates, this process can be aided by bringing the layers into thermal equilibrium using a mild anneal. On other substrates (Si(111)√3 and graphite) no annealing is needed to optimise the crystalline quality of the layers, and sharp quantum well states can be directly observed. Once the layers are of good quality, the development of QWS energies follows the phase accumulation model very well, and binding energies match well to those obtained from first-principle density functional theory calculations.

3.1.2 Quantum Well States in thin In films

Indium shares several physical properties with lead, it is very ductile and has a low melting point for example. It has only one valence electron less than Pb, and due to comparable lattices a similar band structure. Besides this, both metals are non-reactive with the materials used as substrates in this work. A major difference between lead and indium, is the crystal structure of both materials.

Lead has a *fcc* structure, whereas indium has a body centred tetragonal structure. This means that the lattice is contracted about 3 % in one direction, for films grown in the [111] direction, as indicated in the surface Brillouin zone in the inset in Figure 3.15. How this will affect the growth of thin In layers will be discussed in the next chapter concerned with structural interface effects. This lattice distortion has only a limited effect on the electronic structure, as can be observed in Figure 3.15, where DFT band structure calculations for *fcc* and *bct* free-standing indium slabs are displayed. At the zone centre, there is no difference in the QWS energies; differences only occur towards the edge of the Brillouin zone. In the present chapter, concerned with the formation of quantum well states, the changes in electronic structure due to differences in structure will therefore be ignored.

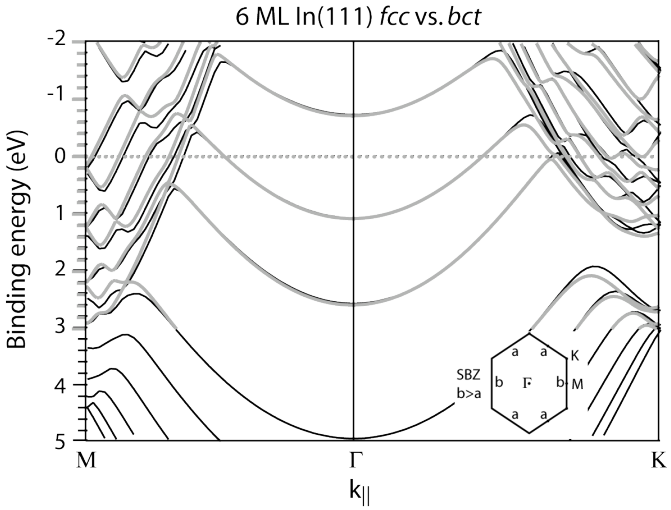

Figure 3.15: Calculated band structure for a 6 ML thick free-standing In slab, with *fcc* lattice structure (black line) and *bct* lattice structure (thick grey line). Note the large similarities around the centre of the SBZ. (inset) SBZ for a *bct* film grown in the (111) direction, with the lattice distortion exaggerated. Calculations from B. Hülsen.

The topmost, partly occupied In valence band crosses the Fermi level at approximately ⅓ of the surface Brillouin zone. Due to the location of this crossing point, a new QWS is expected to appear in the upper valence band for every increment of three atomic layers of indium; this is also reproduced by the QWS energy positions obtained from first principle DFT calculations displayed in Figure 3.16. At a coverage of 3 ML there is only one QWS at a binding energy of 2.0 eV, at 6 ML there are two QWS, and at 9 ML a third QWS is present. It seems that, although for every three monolayers an extra QWS occurs, the first QWS in the upper valence band becomes occupied in

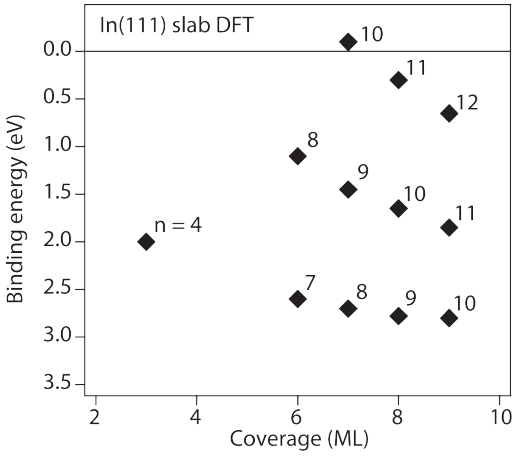

Figure 3.16: Calculated QWS binding energies as a function of layer thickness for free-standing In slabs, with the quantum numbers indicated. From B. Hülsen

a 2 ML thick indium layer. This is reflected in the fact that the third QWS drops below the Fermi level at a coverage of 8 ML and not at 9 ML. In contradiction to the development of the QWS with coverage in the Pb layers, the QWS in the indium layers that have a binding energy close to each other only differ in their quantum number by one. The quantum number n of the state at 1.1 eV in the 6 ML film is 8, for the state at 1.45 eV in the 7 ML film $n = 9$, and for the state at 0.3 eV in the 8 ML film $n = 11$. The $n = 8$ state in the 6 ML film and the $n = 9$ state in the 7 ML film are closer together than the $n = 8$ state in the 6 ML film and the $n = 11$ state in the 8 ML film. The second association is the one that is most easily made for the development of the QWS in the Pb films, resulting in the reduced quantum number $p \equiv 3N\text{-}2n$. For the In QWS a reduced quantum number can be defined simply as $q \equiv n\text{-}N$, resulting in branches of constant q that move downward.

Figure 3.17 shows energy distribution curves for clean Si(100) and several depositions of In on Si(100), obtained at a photon energy of 26 eV. For coverages of 8 ML and more, several features are present that are not observed for the clean Si(100) surface. These lines show a strong dependence on the amount of indium that is deposited, which leads to the conclusion that the features are QWS. For the 4.5 ML thick film it is hard to distinguish any clear QWS and to determine their energies. This is most likely caused by the fact that, at this coverage, the layers grow as islands of mixed thickness, resulting in many states very close to each other. The shape of the background at this coverage strongly resembles the one observed for higher coverages. Here sharp features, identified as QWS, are observed down to around 3.5 eV below the Fermi level. Between 3.5 and 4.5 eV there is a gap in the spectra, which corresponds to the bandgap in the Λ-direction for bulk In. Below this gap, some broad lines can be observed. These are expected to originate from QWS in the lower valence band. Figure 3.18 gives a graphical representation of the correspondence between the location of the bandgap in the bulk material and the possible positions of the QWS in a thin layer. For the lower valence band, a new QWS becomes occupied for every layer, therefore the states are close together and cannot be well resolved. The bandgap does, however, show up clearly

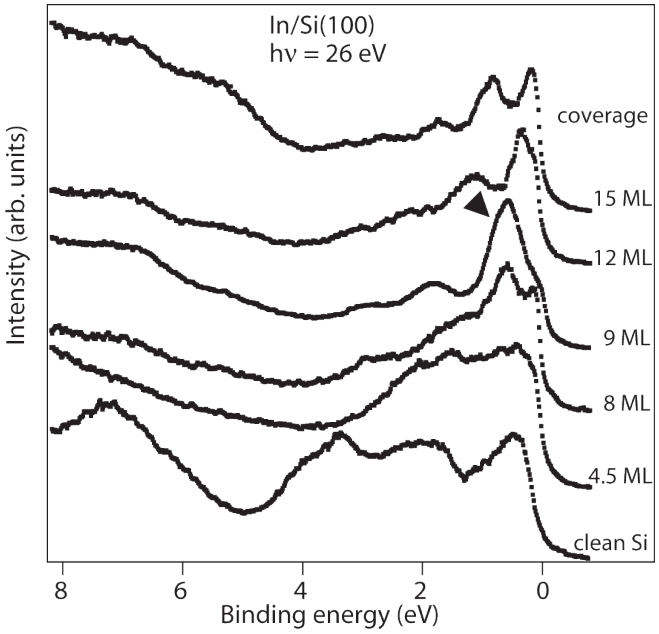

Figure 3.17: Valence level spectra of In on Si(100) for several coverages deposited at 50 K, obtained at normal emission with a photon energy of 26 eV. The black triangle indicates the shoulder on the high binding energy side for the 9 ML film.

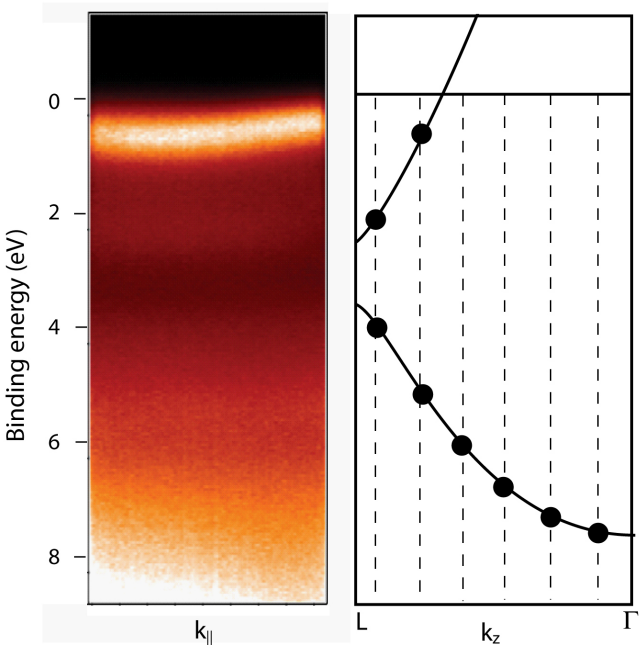

Figure 3.18: (left) Photoemission image of a 6 ML thick In layer on Si(100) obtained away from normal emission at a photon energy of 28 eV. Between 3.5 eV and 4 eV binding energy a dark region can be observed. This corresponds to the bandgap in the bulk band structure of In in the (111) direction (right). For clarity the QWS energies from cutting up the bulk bandstructure are displayed.

in the image. From this figure it is clear that QWS are also formed in the lower valence band of indium; however, since these states are not well resolved due to lifetime broadening, they will not be discussed any further in this work.

The QWS peaks in Figure 3.17 sometimes show a slight shoulder, especially for the first peak in the 9 ML thick film. On the higher binding energy side, a shoulder can be seen that belongs to the 10 ML thick film, as indicated by the triangle. This indicates that the coverage is slightly above 9 ML, and therefore areas with a 10 monolayer coverage exist. Such features will be taken into account in the evaluation of the data in order to more accurately determine the energies of the main features in the spectra. Figure 3.19 shows the binding energy positions for the most prominent QWS in thin In layers on Si(100) as a function of coverage. The measured energies are indicated by solid triangles, while the QWS energies obtained from DFT calculations are indicated as open circles. It is clear that the QWS obtained after deposition of 8 ML of indium do not match with the calculated results. The energies of the unoccupied QWS are obtained by extrapolating the peak that is visible at the Fermi level, and is therefore cut off. From a comparison with the binding energies obtained by DFT, the QWS measured for a 8 ML thick film can be ascribed to a combination of a 7 and 9 ML thick film. This means that the 8 ML film is not formed at all! A possible explanation for this will be given in the second part of this chapter. When the QWS observed for the 8 ML film are appropriately assigned, as indicated by the arrows, the measured energies follow the calculated ones perfectly, especially when the branches of constant q are extrapolated. It can therefore be concluded that indium grows in a layer-by-layer fashion for coverages of 9 ML or more. It seems that below this coverage, a mixture of layer heights is formed, which is confirmed by the data for both the 4.5 and 8 ML depositions. This is comparable to the “inverse Stranski-Krastanov growth”

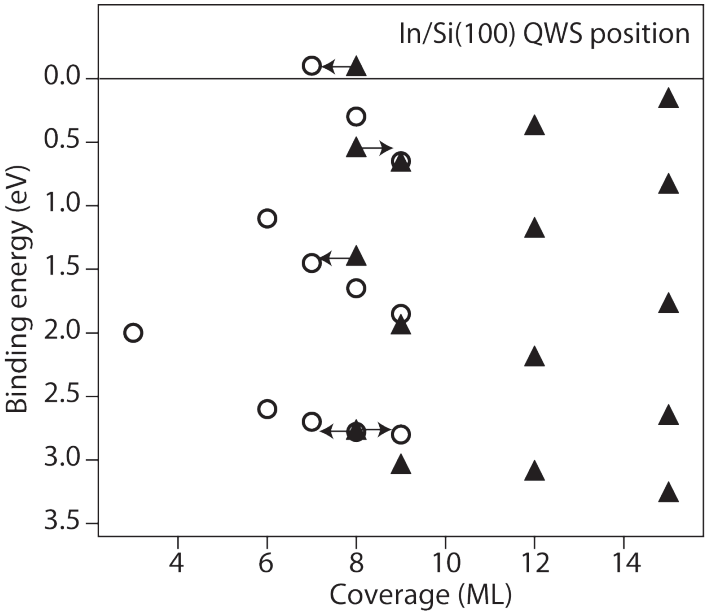

Figure 3.19: Quantum well state binding energies as a function of coverage, for In/Si(100) from photoemission measurements (triangles) and from DFT calculations (circles). The arrows indicate that for a coverage of 8 ML, the layer will consist of a combination of 7 and 9 ML heights.

observed for Ag on GaAs(110)[14] where, as discussed in Chapter 2, after initial island growth from a certain coverage onward atomically smooth layers are formed.

In the analysis of the quantum well states in thin Pb layers shown in the previous section, it became clear that it is important to examine the QWS energy positions as a function of photon energy in order to distinguish any bulk-like features from the QWS. Figure 3.20 shows the photon energy dependence of the QWS in a 15 ML thick indium film on Si(100), from 16 to 34 eV photon energy. The individual spectra are obtained by taking a slice through an "energy versus angle" image at normal emission, the spectra were then normalised to the mirror current of the beamline. Two clear observations can be made from this figure. First, the QWS show no noticeable dispersion as a function of photon energy, again confirming the confinement of wave functions in the direction normal to the film surface. Secondly, there are strong variations in the intensity of the QWS as a function of photon energy. At $h\nu = 16$ eV the QWS are not distinguishable above the background and noise level, a clear Fermi edge is also not developed. Above a photon energy of 18 eV the Fermi edge and QWS start to become visible, the intensity continues to increase until around 29 eV. After this photon energy, a behaviour occurs that is comparable to the results for the annealed and well ordered Pb films. The weight of the QWS intensities shifts away from the Fermi level, and follows the dispersion of the bulk band. Due to this direct transition, the intensity of the quantum well states close to the Fermi level decreases relative to the deeper lying states. From this plot an optimum photon energy that combines a high cross section with a broad energy window in the analyser can be determined. This optimum is located around 26 eV, hence this is the photon energy that was used in the rest of the experiments involving thin indium layers.

14 A.R. Smith *et al*, Science **273**, 266 (1996).

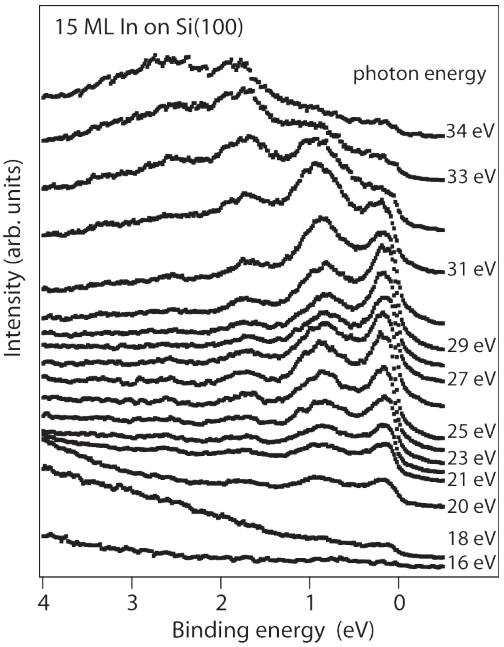

Figure 3.20: Energy distribution curves for a 15 ML thick layer of In on Si(100) at 50 K as a function of photon energy. The spectra have been normalized to the mirror current.

For indium deposited on Si(111)7x7, the energy distribution curves are shown in Figure 3.21. The bottom spectrum is for clean Si(111), where two surface states can be observed; the adatom-derived S_1 at a binding energy of 0.2 eV, and the restatom-derived S_2 at $E_B = 0.8$ eV[15], as indicated in the plot. For six layers of indium, the Fermi edge is well developed, but only broad features are present in the valence band. The image from which this spectrum has been extracted (Figure 3.22), still shows the downward dispersing silicon valence band. Directly above this sharp feature, a broad band can be observed that shows no dispersion with polar angle. This is also the broad peak that shows up in the EDC for 6 ML in Figure 3.21. The fact that the silicon valence band is still clearly visible leads to the conclusion that, just as on Si(100), the indium grows in islands for

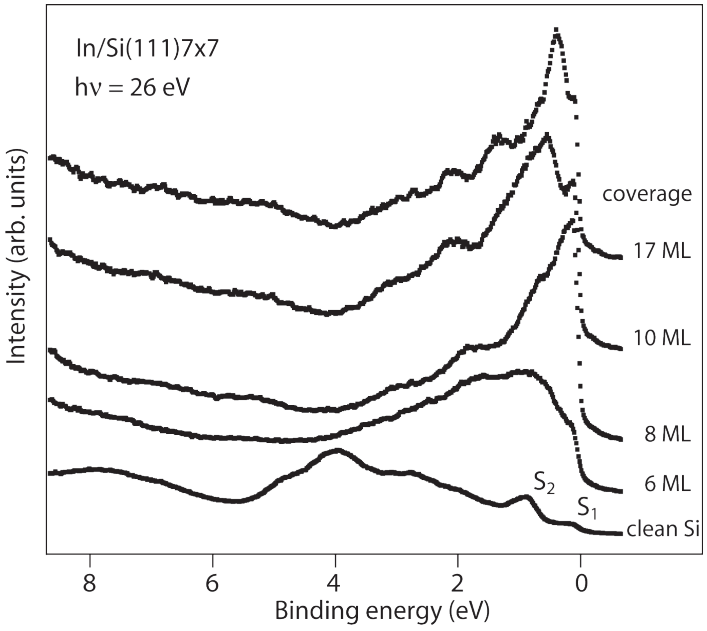

Figure 3.21: Valence level spectra of In on Si(111) for several coverages deposited at 50 K, obtained at normal emission with a photon energy of 26 eV. The adatom-derived S_1 and the restatom-derived S_2 surface states for the clean Si(111) are indicated in the plot.

15 R.I.G Uhrberg et al. Phys. Rev. B, 31, 3805 (1985); R.J. Hamers et al. Phys. Rev. Lett. 56, 1972 (1986).

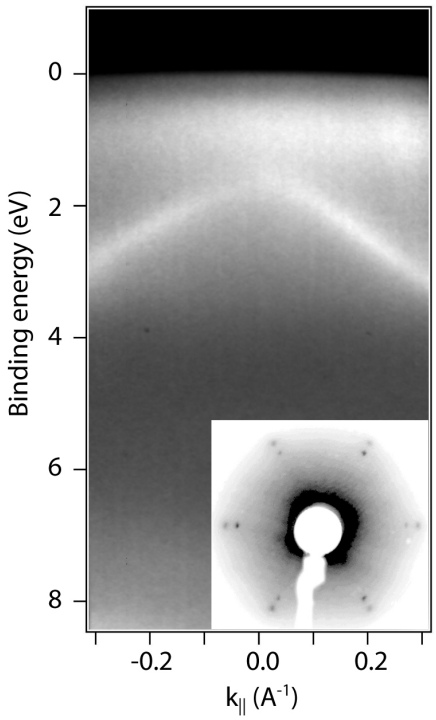

Figure 3.22: Binding energy vs. $k_{||}$ photoemission image for 6 ML of In on Si(111) deposited at 50 K, obtained at a photon energy of 26 eV. (inset) LEED pattern for the same sample at a electron energy of 85 eV, showing both diffraction from the In islands (outer spots) and the Si substrate (inner spots).

these low coverages. This is confirmed by the LEED image for this coverage, shown in the inset in Figure 3.22. The inner spots, originating from the Si(111) surface, are more intense than the indium spots, which due to the difference in lattice spacing show up just outside the Si spots. This island-like growth has been confirmed in STM studies by Altfeder *et al*.[16], who also determined that the islands are slightly elongated in the direction along the step edges due to lack of diffusion perpendicular to the steps.

For coverages of 8 ML or more, it seems that the islands close to form a smooth layer. Individual QWS can be clearly resolved, and these states show a strong dependence on the total coverage. The gap just below 4 eV binding energy, as in In/Si(100), can be clearly observed. A major difference, however, is the intensity difference between the QWS within approximately 1 eV below the Fermi level and the deeper lying states. For In/Si(100), the QWS intensity only showed a gradual decrease away from E_F, whereas here it is very abrupt. This cannot be a matrix element effect, because both data sets have been recorded at the same photon energy; the matrix elements will not change between the two systems because both films grow in the [111] direction. This discrepancy is therefore attributed to interface effects, as will be explained in Chapter 4.

Figure 3.23 shows the binding energy position of the primary QWS extracted from the EDC in Figure 3.21. Because of the relatively large gap in the coverage between 10 and 17 ML, lines of constant *q* are drawn for clarity. It can be directly concluded that indium layers grown on Si(111) also follow the general trend predicted by DFT and observed for In/Si(100). For every three additional monolayers deposited, one additional QWS is formed in the upper valence band.

16 I.B. Altfeder et al. Phys. Rev. Lett. **92**, 226404 (2004).

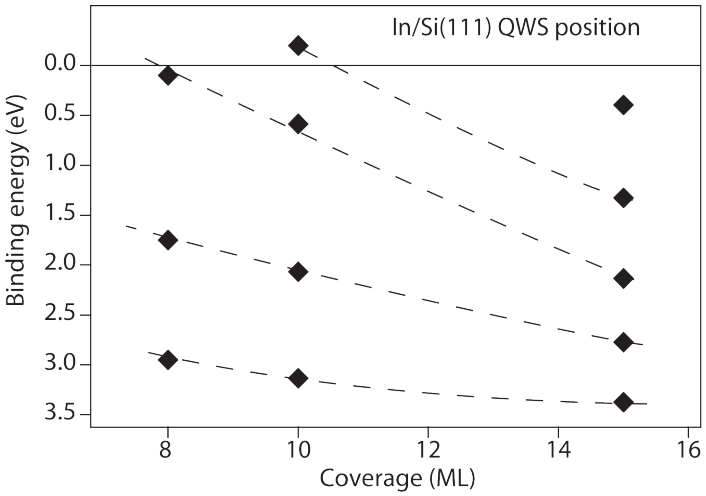

Figure 3.23: QWS binding energy as a function of coverage for In layers on Si(111) deposited at 50 K. The dashed lines indicate the branches of constant q.

3.1.3 Quantum Well States in thin Al films

The formation of quantum well states in thin aluminium films has been extensively discussed[1] previously, primarily for growth on Si(111) and Si(100). In these experiments by Aballe and coworkers, it was observed that atomically smooth layers of Al can be formed by first depositing at low temperature and then annealing the system to room temperature. Figure 3.24 shows a deposition series of Al on Si(111)7x7 before and after annealing (Ref. 1). The result of the anneal is clear, and the energies and spacing of the individual QWS indicated that there is no mixture of coverages. Annealing of the layer is necessary in these experiments, because upon initial deposition the crystalline structure at the interface between the aluminium and the silicon is not well defined. After annealing, the interface between the silicon substrate and the Al overlayer is well ordered, such that coherent backscattering of the electrons can occur, and standing waves are formed.

This annealing procedure to obtain a crystalline layer is beneficiary on different substrates, as shown by the data in Figure 3.25. Here an annealing sequence is shown for a 17 ML thick aluminium film deposited on the single crystal graphite surface at 100 K. In the bottom spectrum, for the as-deposited layer, hardly any features can be discriminated. The Fermi edge is, however, well developed, suggesting that the whole surface is covered. This is confirmed by the LEED pattern obtained from this layer (Figure 3.26(a)). No substrate spots are observed in this situation. The LEED pattern of the

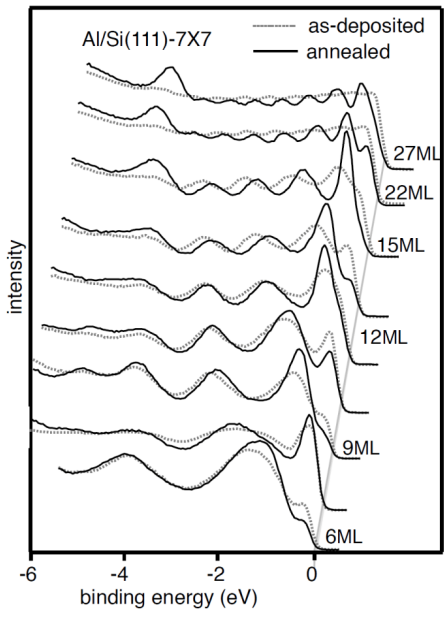

Figure 3.24: Photoelectron spectra of Al layers on Si(111)7x7 as-deposited (grey traces) at low temperature and after annealing to the optimum temperature (black traces). Figure from Aballe[1].

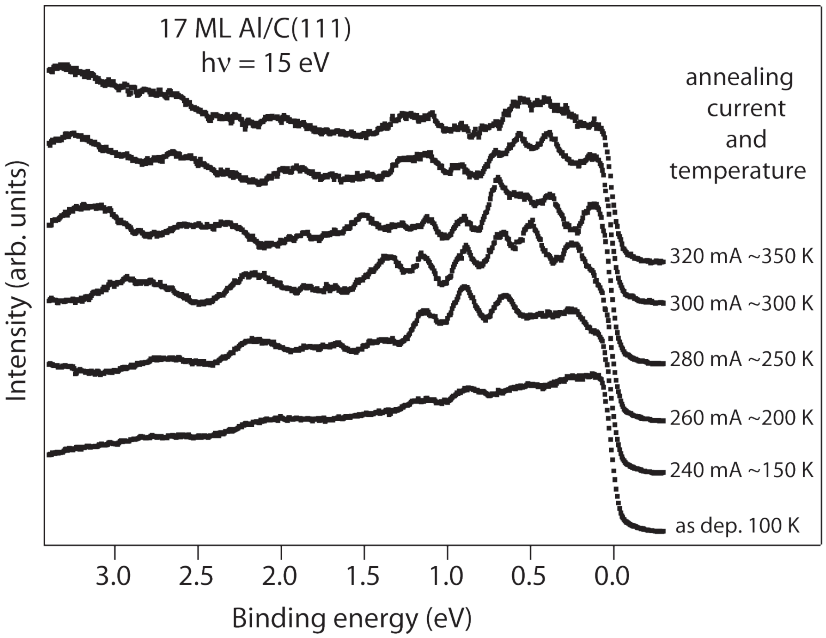

Figure 3.25: Energy distribution curves for 17 ML of Al on graphite as a function of annealing current and approximate temperature. The spectra have been obtained at normal emission at a photon energy of 15 eV.

aluminium layer is composed of a very narrow ring with a six-fold intensity modulation. This indicates that, although the aluminium layer is composed of crystalline [111] facets in the upper atomic layers, it grows in a rotationally disordered fashion. In order words, the film is composed of a large number of slightly rotated domains.

Upon annealing the layer, sharp features show up in the valence band, which are not present in the substrate or in bulk aluminium. In Figure 3.25 the annealing steps are indicated by the current through the SiC substrate, and approximate temperatures. For currents below 240 mA there is no change in the valence band, and the respective spectra are therefore not displayed. With every further annealing step, new features appear in the valence band; of these, the three peaks at approximately 0.65, 0.90 and 1.15 eV appear for all annealing steps. These three QWS peaks cannot belong to the same coverage, because this would mean that further QWS would have to occur at around 0.4, 0.15, and 1.4 eV. Here an approximately equidistant energy spacing between the QWS is assumed, which is a very good approximation in this energy range. If the two outer peaks would originate from the same coverage, following the same argument as above, further QWS would have to appear at 0.15 and 1.65 eV with similar intensities. This is obviously not the case, which leads to the conclusion that all three features belong to a different layer thickness. Combining this with the LEED obtained after annealing the sample at 260 mA (Figure 3.26(b)), it is clear that the layer has broken up into islands of different height. The spots from the bare graphite substrate reappear outside the ring from the Al overlayer. The fact that this ring is still present indicates that the reorganisation of the Al islands primarily occurs by changing their height, and by creating a good crystalline structure perpendicular to the surface. The individual islands all keep a different rotational orientation, and the orientation of the underlying graphite substrate is only slightly preferred. This is different from the case of Pb on graphite, where the in-plane orientation of the Pb islands follows that of the graphite (Figure 3.12(a)).

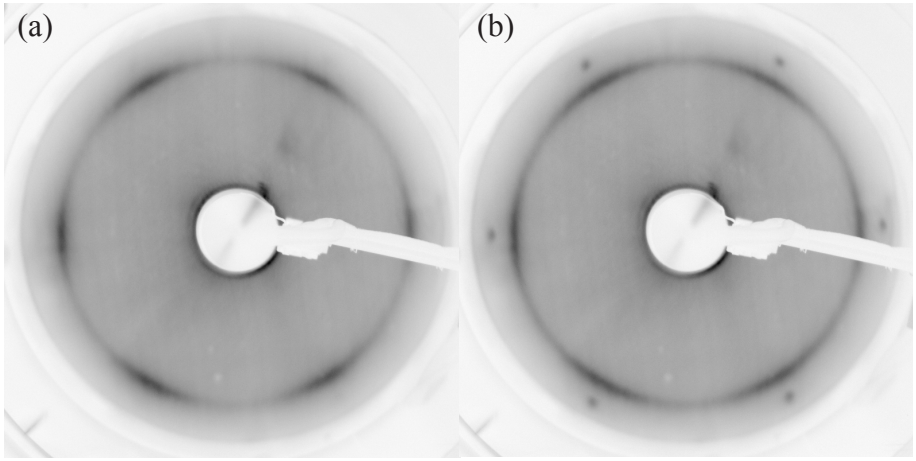

Figure 3.26: LEED pattern of 17 ML of Al on graphite obtained with an electron energy of 90 eV for the as-deposited layer (a), and after annealing at 260 mA (b). The sharp spots in (b) are from the graphite substrate, indicating that the layer breaks up in islands.

The fact that the islands do not have the same in-plane orientation, does, however, not lead to a broadening of the width of the peaks. Figure 3.27 shows a comparison of valence band spectra obtained from a typical 17 ML thick layer of aluminium on Si(111) after anneal, and the Al islands on graphite after a similar anneal. From the width of the Fermi edge it can be concluded that the energy resolution for both spectra is the same. For the Al/Si(111) spectrum this Fermi fit is shown, with a width of 98 meV. This makes the difference in width of the QWS even more striking. The QWS measured for Al/Si(111) are more than four times as broad as those observed in Al/C. This difference makes a comparison between the two systems, in order to extract the island heights for Al/C, very difficult. It is likely that one peak in Al/Si(111) is actually composed of three or four QWS from different coverages, comparable to observations for Pb/Si(111)7x7 above. In order to circumvent this problem, a comparison to theoretically expected QWS binding energies in Al(111) is necessary. In order to achieve this, the bulk band of Al in the [111] direction has been parameterized and fitted with a third degree polynomial. From this modelled band the QWS energy positions can be obtained in a similar way as in Figure 1.9, thus extracting the binding energy at $^{i}/_{N}$ part of the full Brillouin zone, where N is the number of monolayers, and i an integer running from 1 to N. The result of this approach is shown in Figure 3.28. Deviations from DFT calculations are primarily expected towards the bottom of the band, because here the band is difficult to parameterize; this would shift the QWS in this energy region towards higher binding energies by a small amount.

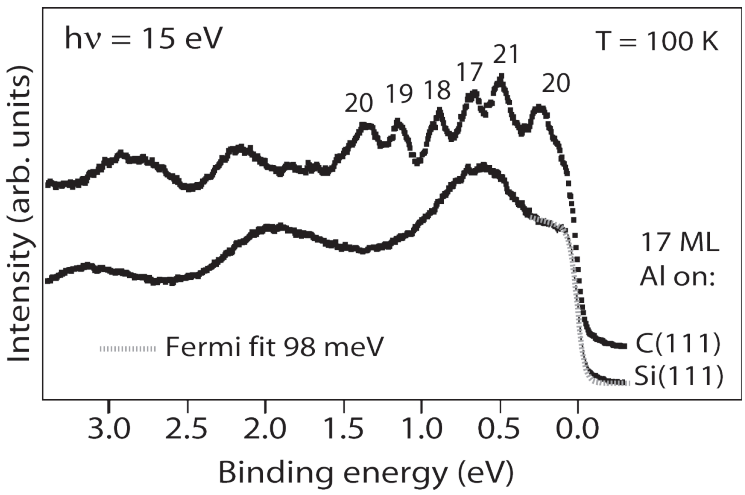

Figure 3.27: Energy distribution curves for 17 ML of Al on graphite and on Si(111)7x7 obtained at 100 K after first annealing the layer to room temperature. For the Al layer on Si the Fermi function with a width of 98 meV is shown. Both spectra are measured at normal emission at a photon energy of 15 eV. The numbers near the Al/C spectrum indicate the island heights that the QWS are derived from, see text for details.

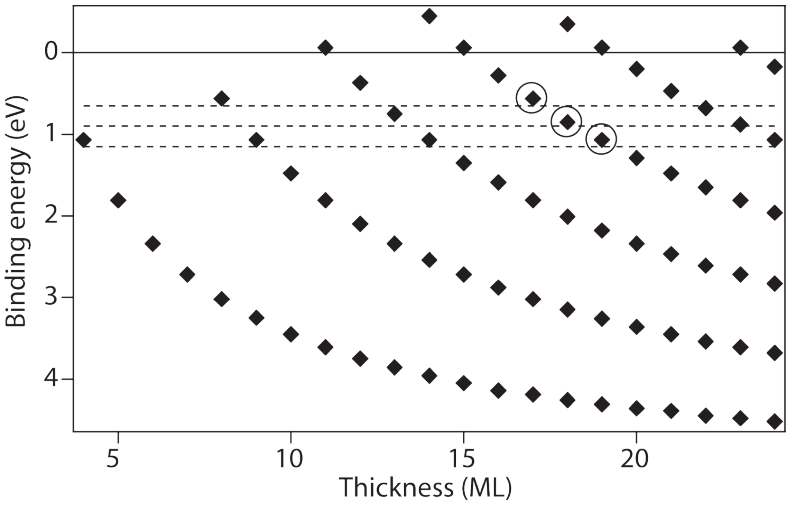

Figure 3.28: QWS binding energy positions for Al as a function of layer thickness, obtained from the bulk Al band structure as described in the text.

As with every simple theoretical approach, discrepancies with measured data are to be expected. However, in all its simplicity the model provides a good starting point in the energy region of interest here. The three horizontal dashed lines in Figure 3.28 represent the QWS energy positions measured after annealing the layer at 240 mA. Incorporating the fact that the initial deposition was approximately 17 ML, and that after annealing the substrate becomes visible, the QWS can be identified as originating from 17, 18, and 19 ML high islands. After the next annealing step the island heights expand to include islands of 20 and 21 ML atomic layers high, corresponding to the QWS at 0.23, 0.5, and 1.36 eV.

The mixture of many rotational domains is expected to have a profound effect towards the edge of the surface Brillouin zone, because here a mixture of bands for the Γ-M, Γ-K and all directions in between would show up. This is confirmed by the in-plane measurement for the layer after annealing to 260 mA, shown in Figure 3.29. In the centre of the image, the QWS are very sharp, but towards the edge they become more vague. That this is not due to measurement conditions can be confirmed from the similar measurement for Pb on graphite in Figure 3.11, where the features remain sharp well into the second SBZ. A striking observation from Figure 3.29 is the transition from a region where the QWS are sharp, to an energy region where they become broader. This change occurs somewhere between 1.5 and 2 eV, and is not gradual enough to be solely caused by

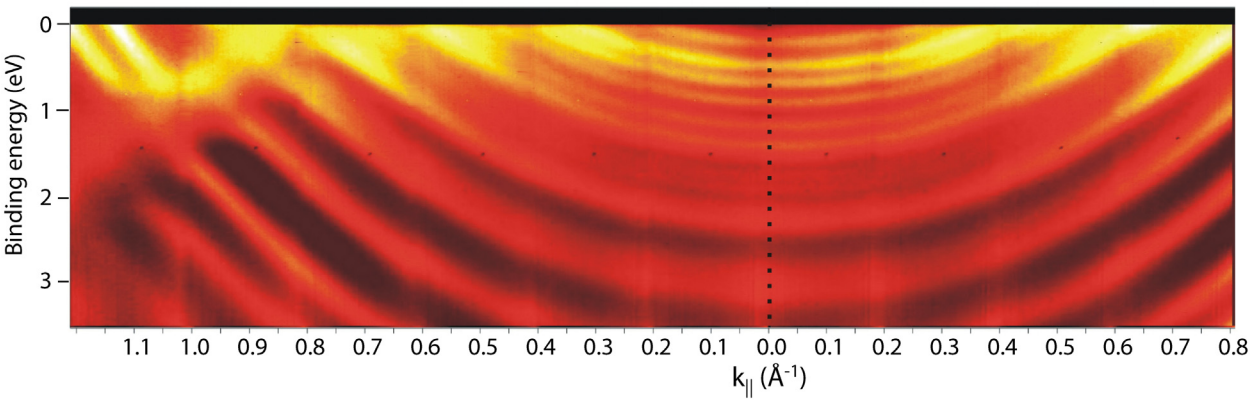

Figure 3.29: Cut through the SBZ for 17 - 21 ML high Al islands on graphite obtained at a photon energy of 15 eV. The dashed line indicates normal emission. Note that close to E_F the states are very sharp and that they become broader further away. The features around 1 $Å^{-1}$ are the $3p_{x,y}$ states dispersing down from high above E_F.

life-time broadening effects. Although not previously reported, this is actually an inherent property of quantum well systems where a mixture of adjacent layers is present. The change in sharpness is caused by the difference in slope of the branches close to the Fermi level, and further towards the bottom of the band. In order to illustrate this effect, the QWS energies expected to occur for aluminium layers with thicknesses between 17 and 21 ML have been broadened by a Gaussian with a width of 0.1 eV and unity intensity. The used width is comparable to, and even slightly larger than, experimental observations for the QWS closer to the Fermi level in this system. The result of this model, multiplied by a Fermi function with a width of 80 meV, is plotted in Figure 3.30, together with an experemtally obtained EDC. Although the exact energy positions are not reproduced for the higher binding energy features, the correspondence to the spectra shown in Figure 3.25 and the image in Figure 3.29 is striking. In the first 1.5 eV below E_F, sharp individual QWS can be resolved. Between 1.5 and 2.5 eV there seems to be a transition region, the sharp states can been seen to dissolve into larger peaks. Below 2.5 eV the individual QWS can no longer be resolved, but it is clear from the model, that the peaks around 3 and 4 eV are composed of 5 smaller peaks. Between these large composite peaks, there is no intensity from either of the 5 different island heights, and these peaks can easily be mistaken for individual QWS belonging to a single coverage.

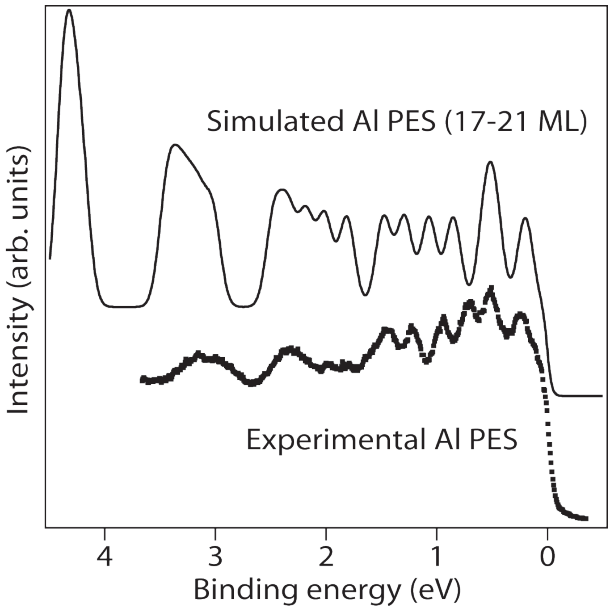

Figure 3.30: Simulated and experimental photoemission spectrum for a mixture of Al island heights from 17 to 21 ML. The QWS binding energies from Figure 3.28 have been modulated with a 0.1 eV wide Gaussian and multiplied with a 80 meV wide Fermi function. Note that the features are narrow close to E_F and become broader for higher binding energies.

The fact that these observations, which are be typical for all quantum well systems of s-p-metals, can be made, is due to two main factors. First, a system is needed that allows for the formation of QWS with a Gaussian width of less than 0.2 eV. From the data obtained for Pb/Cu(111), Pb/Si(111)7x7, In/Si and Al/Si(111), it is obvious that such sharp features are not typical for metallic quantum well systems. Secondly, a sudden change in sharpness of the features will only show up when several adjacent heights are present simultaneously. For Pb on Si(111)$\sqrt{3}$x$\sqrt{3}$ and on graphite, the states are equally sharp, but either atomically flat layers are formed, or islands of several non adjacent heights.

In conclusion, the data in this section shows for several systems, that have not been studied before, that the formation of metal layers that can accommodate quantum well states is successfully achieved. Due to the high resolution angle-resolved photoemission measurements the important characteristics of these states could be determined with high accuracy. The change in binding energy position as a function of layer thickness is studied extensively, and is matched to a picture where the bulk band structure of the metal is "cut up" due to the confinement of the electrons. For Pb and In films the obtained results are compared to density functional theory calculations for free-standing films, in which also parameters as spin-orbit coupling and lattice distortion are included. These calculations are used to identify the orbital character of the QWS, which is essential in order to obtain a complete understanding of the band structure. The growth of atomically flat layers or islands is achieved for all systems presented here, and the growth-mode of the overlayers is characterised, based solely on ARPES and LEED results. For the Pb and Al films on graphite, QWS are measured with a peak line width in photoemission up to four times smaller than previously reported. The data for Al/C(111) show that layer resolved QWS can still be resolved close to the Fermi level, even when the system consists of a mixture of 5 different island heights. Cuts through the surface Brillouin zone are shown for Pb and Al on graphite which exhibit an excellent correspondence to calculations, indicating the formation of quasi free-standing films on the graphite substrate.
For Pb films on Si(111) and Cu(111) a bulk-like feature is identified in the photoemission spectra, the origin of this feature is briefly explained. Moreover, it is shown how this feature can be distinguished from the QWS, something that will prove crucial further on in this thesis. Both for thin Pb and In layers the dependence of the features in the photoemission spectra show strong matrix element effects; i.e. the photoemission intensity envelope follows the direct transition of the bulk material. Along these lines, an optimal photon energy can be determined for photoemission measurements on a quantum well system, based only on measurements of the bulk material.

3.2 Influence of the electronic on the atomic structure: Electronic growth

In the previous section, I have discussed how the reduced dimensionality of thin metal overlayers leads to the formation of quantum well states, and have interpreted their properties in detail. One of the characteristics of these states is that their energies depend on the layer thickness. In a first approximation, the total energy of a thin metal layer is proportional to the energy of the highest occupied QWS at the SBZ centre[17]. From the results discussed in the previous section it is

17 D.-A. Luh *et al*, Science **292**, 1131 (2001).

therefore clear that the total energy of the layer will depend on its thickness in a complex manner. The concept of electronic growth, introduced by Zhang[18], is based on these variations in film energy. In this section it will be shown that the dependence of total energy on the film thickness can have a profound influence on the growth of metallic overlayers, a consideration that may have implications for applications in technology.

For Pb on Cu(111) it was shown in Figure 3.4 that annealing of the deposited Pb layer induces remarkable changes in the valence band spectra. These changes are associated with the formation of single height islands, whereby also the crystalline structure of the layer is improved. A considerable amount of additional information can, however, be inferred from this data set. The as-deposited films (dashed lines) exhibit clear peaks in the density of states that extend right up to the Fermi level, see for example the 8.5, 10.5, and 14 ML thick films. Upon annealing, two processes can happen; either an existing peak increases and the other vanishes, or a entirely new peak occurs (17 ML). In either case, features with a spectral weight at higher binding energies now dominate the spectra. As discussed previously, the new spectra can be explained in terms of a severe morphology change. Because the growth mode at low temperature is layer-by-layer for this system, the structural change cannot lead to lower coverages. Therefore, if a structural change towards higher island heights occurs, more of the bare substrate should contribute to the PE signal, since some regions would be deprived of overlayer material. In photoemission, this can be probed by measuring the signal from a substrate line such as the Cu 3d lines before and after annealing. Such data are shown for the 5.6 to 19.5 ML thick films in Figure 3.31. In the upper part, the dashed lines represent the spectra for the as-deposited layer, and the solid lines those obtained after the layer has been brought into thermal equilibrium. From this plot two conclusions can be drawn: first, substantial regions of the Cu substrate are exposed or are burried underneath a thinner layer of Pb as a result of the annealing. Secondly the amount of increase depends on the initial coverage. The latter is more clearly illustrated in the bottom part of Figure 3.31, here the Cu 3d line increase is depicted as a percentage of the initial signal, as a function of coverage.

At first glance, the observation that the topmost QWS shifts away from the Fermi level, and the variations of the increase in the Cu 3d signal, do not seem to be related. They do, however, have the same physical origin, which is the tendency to minimize the total energy of the layer. This observation can be explained better if we first consider this on a more quantitative level by analysing the peak energies in the spectra from the as-deposited and annealed films. The observed peak energies are indicated and assigned to their respective layer thicknesses according to the phase accumulation model, in Figure 3.32. The obtained QWS energies are compared to results from two models: first the DFT results from Wei and Chou[19] (solid lines), and further to considerations of

18 Z. Zhang *et al*, Phys. Rev. Lett. **80**, 5381 (1998).

19 C.M. Wei and M.Y. Chou, Phys. Rev. B **66**, 233408 (2002).

the energetics of QWS based on the measured Fermi surface of Pb by Otero *et al*.[20] (circles). The correspondence between the experimental results and the predicted binding energies is very good, especially at higher coverages. This is primarily due to the fact that the interface was not incorporated into the model, and that its relative influence will diminish when the layer gets thicker, as discussed above. The triangles represent the observed QWS energies for the as-deposited layer, and the squares the measured energies after annealing the sample. The arrows indicate an increase or decrease of the layer thickness. The 9 ML as-deposited layer, for example, will bifurcate into 8 and 10 ML high islands. In agreement with results from the individual spectra, all the arrows point towards higher binding energies, again indicating a shift of density of states away from the Fermi level. The thicknesses that result after annealing the layer can be regarded as the "preferred" heights, corresponding to the nomenclature introduced in Chapter 1. From this analysis I conclude that the preferred heights for Pb on Cu(111) are 6, 8, 10, 15, 18, and 22 ML. At these coverages the topmost occupied QWS is furthest away from the Fermi level in that coverage range. The increase in the Cu 3d signal, which is directly related to the amount of Pb that is moved from lower to higher coverages, can then be related to the difference of the initially deposited amount to the nearest stable height. When the difference between this optimal thickness and the deposited amount is large, a large amount of material is moved and the increase in Cu 3d signal will also be large. For this reason the general trend of the Cu 3d line increase as a function of coverage, follows a sawtooth like behaviour.

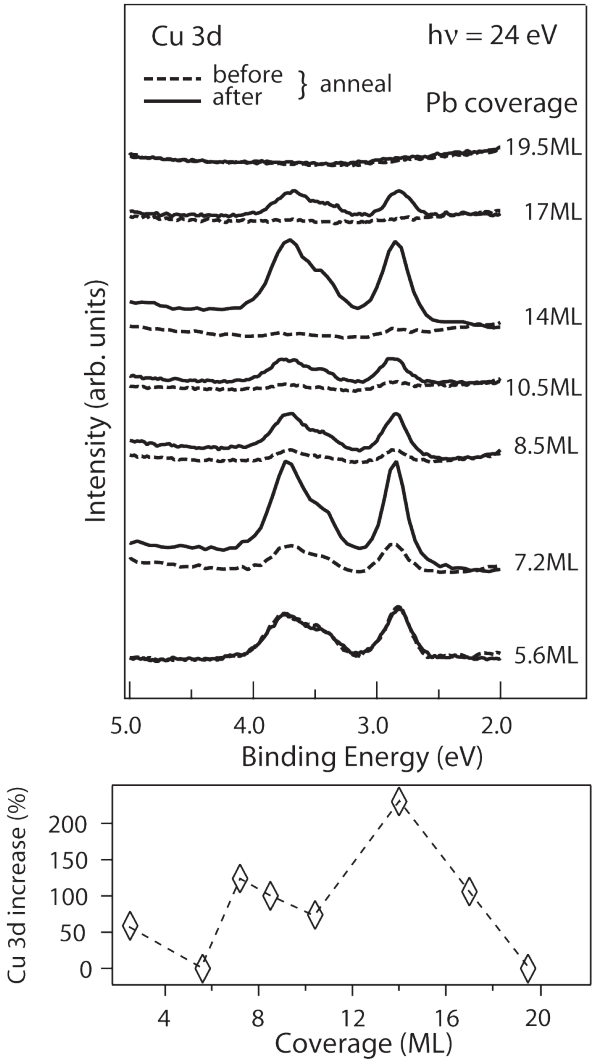

Figure 3.31: (top) Photoemission spectra in the energy region of the Cu 3d lines obtained at normal emission at a photon energy of 24 eV. The dashed lines represent the as-deposited layer, and the solid lines the annealed layer. (bottom) Increase in the Cu 3d signal as a percentage of the initial signal. The dashed line connecting the points is intended as a guide to the eye

Such changes in island height have to be accompanied by a considerable mass transfer of Pb to the top of islands. From the sharp spectral shape of the QWS in photoemission, and from STM

20 R. Otero, A.L. Vazques de Parga, and R. Miranda, Phys. Rev. B **66**, 115401 (2002).

measurements[20], comparable to those shown in Figure 3.33[21], it is concluded that the resulting islands have steep edges and flat tops. The relatively fast diffusion of Pb atoms to the top of 100 Å high islands, is confirmed by STM data from Okamoto *et al*[22]. The same stabilising principle that is responsible for the formation of preferred layer heights, is also the cause for the formation of these flat-topped islands. An alternative way of treating the formation of stable heights is to consider the mismatch between the electron wavelength and the height of the island. At the preferred heights, exactly an integer number of electron wavelengths will fit into the layer thickness. If there were regions on the top of the islands where the is one atomic layer more (or less) present, or where there is atomic roughness, the mismatch would dramatically increase. This would lead to a locally large charge spilling out of the surface, which is an energetically unfavourable situation. In other words, it can be said that the standing electron waves form a stabilizing mechanism against roughening of the top of the islands.

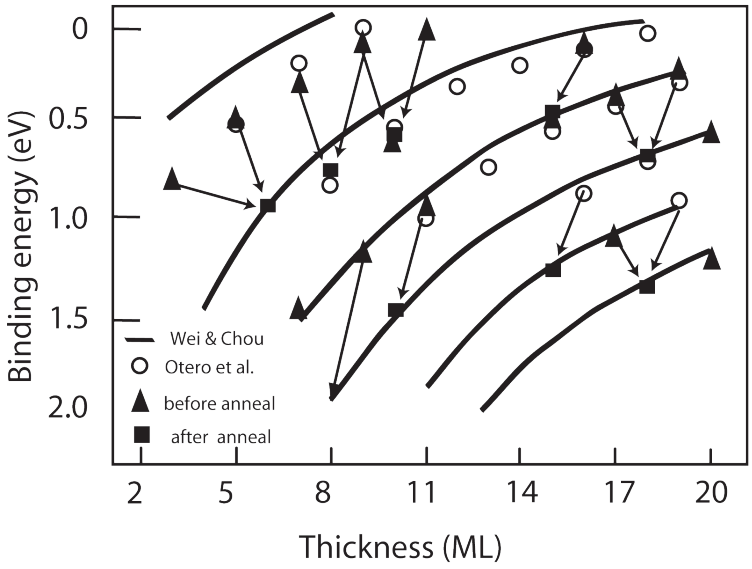

Figure 3.32: Energies of quantum well peaks for different Pb coverages, derived from calculations within the phase accumulation model, (lines) DFT calculations (Wei and Chou), (circles) an infinite potential well model (Otero et al.), and from the photoemission data in Figure 3.4, (triangles) before anneal, and (squares) after anneal.

The preferred stable heights measured in this experiment correspond very well with the STM results presented by Otero *et al.*[20], where preferred heights are observed for 6, 8, 10, 11, 15, and 17 ML. However, the 11 monolayer high island turns out to be very unstable from the results presented here, and will disproportionate into 10 and 15 ML islands when annealed. The reason for this discrepancy between the STM and these photoemission results, can be found in the fact that at 11 ML, a state is predicted to be exactly straddling the Fermi energy. This state will, depending

21 M. Hupalo *et al*, Phys. Rev. B **64**, 155307 (2001).

22 H. Okamoto, D. Chen, and T. Yamada, Phys. Rev. Lett. **89**, 256102 (2002).

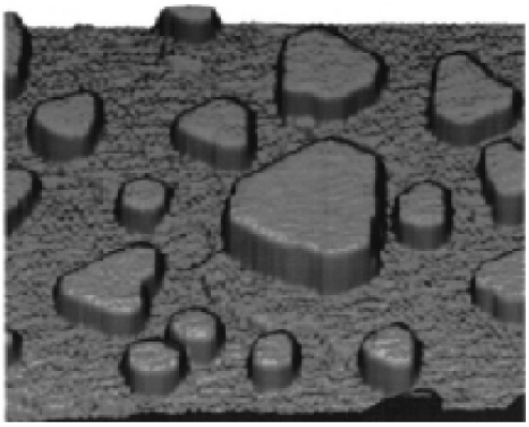

Figure 3.33: STM image of magic height Pb islands on Si(111)√3 showing flat top islands with steep edges. Image from Hupalo[21].

on the exact interface configuration, either fall just above or below E_F, yielding an energetically favourable or unfavourable situation influenced by just a small change in the boundary conditions at the interface. This is confirmed by Otero *et al*. in the observation that the density of step edges has a strong effect on the observed preferred heights. A similar line of reasoning may explain why in this study, a preferred height is observed for 18 ML islands, whereas the STM results yield 17 ML as a preferred height. The next branch of quantum well states with reduced quantum number *p*, passes through the Fermi level around 18 ML. Note that Otero *et al*. use room temperature deposition, whereas here deposition at 100 K is followed by annealing. It is well known that the details of the preparation recipe can have a pronounced influence on film morphology[23].

As discussed above, the formation and the exact height of magic layers depends on the exact interface structure. This is also confirmed by the fact that on the 7x7 reconstruction of Si(111), 8 ML thick films are most stable, whereas on the √3x√3 reconstruction 6 ML high islands are predominantly observed[24]. To allow for a comparison with photoemission data, the wetting layer has already been incorporated in these heights. In Chapter 1 this difference has been explained by considering the total energy calculations for Pb layers on the two interfaces (Figure 1.9). The position of the relative energy minimum is at 8 ML on the 7x7 reconstruction, and at 6 ML on the √3x√3 reconstruction. In order to study the influence of the quantization and the formation of standing electron waves, independent of the substrate, one has to consider a film that is decoupled from the substrate. In section 3.1.1 I concluded from the perfect match between calculations for free-standing slabs and the measured electronic structure of the QWS of Pb on graphite that the Pb layers on this substrate are quasi freestanding. This conclusion is supported by the fact that graphite has no bands in the energy region where QWS are formed from the upper Pb valence band. Moreover, there is no chemical interaction between the Pb layers and the graphite, and Pb does not form a wetting layer on this substrate. Therefore, this system provides a perfect basis for the study of the formation of "magic" heights independent of a substrate, and a tool to test theoretical predictions.

23 L. Aballe, C. Rogero, and K. Horn, Phys. Rev. B **65**, 125319 (2002).

24 V. Yeh, L. Berbil-Bautista, C.Z. Wang, K.M. Ho, and M.C. Tringides, Phys. Rev. Lett. 85, 5158, (2001).

Figure 3.13 showed that for coverages until at least 7 ML, only 2, 4, 6, and 8 ML high islands are formed. Although this derivation was from layers that were not annealed, due to the low diffusion barrier for Pb on graphite even at 100 K, the resulting island heights can be regarded as preferred heights. Furthermore, from the fact that certain heights (for example 3, 5, and 7 ML) are not formed, these can be concluded to be unstable. The 6 and 8 ML high islands are those that are magically stable on Si(111)√3 and 7x7, respectively. For films to become magically stable, there has to be a local minimum in the surface energy of the layer. This surface energy can be modelled by the following damped sinusoidal function[19]

$$\frac{A\left|\sin(k_F\, d\, N+\varphi_0)\right|+B}{N^{\alpha}}+C\ , \tag{3.1}$$

where N is the number of ML, d the interlayer spacing, and k_F the electron wave vector at the Fermi level, measured from the L-point of the Brillouin zone. A, B, C, φ_0, and α are constants independent of layer height. The results of this equation for $\alpha = 2$, are depicted as the open circles and dashed line in Figure 3.34. The calculated values represented by the solid circles are obtained using a generalized gradient approximation. Clear minima in the surface energy are distinguishable for 2, 4, and 6 ML thick layers, which directly corresponds to the island heights formed for Pb on graphitized SiC.

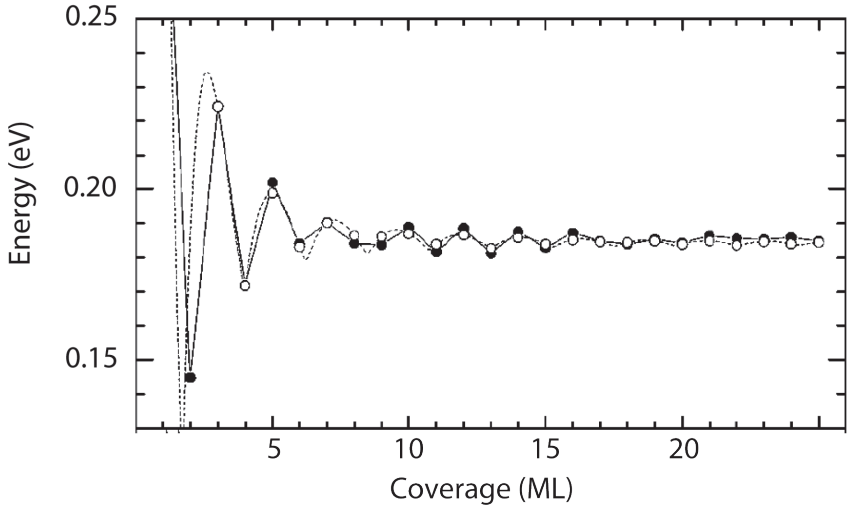

Figure 3.34: Calculated layer energy per site vs. thickness for free-standing Pb films. The dashed line and open circles are from Eq. 3.1, the full circles are obtained using a generalized gradient approximation. Figure from Wei[19].

In the present experiments, a major advantage of the use of angle resolved photoemission is that not only the result of electronic growth, but also its origin can be detected. The result is that only islands of 2, 4, 6, and 8 ML are formed, which can be reasonably well explained by a minimization of the surface energy. The cause for this becomes even more obvious when considering the full in-plane electronic structure as depicted in Figure 3.11. Although the $6p_{x,y}$ bands will cross the Fermi level for every given height, an E_F crossing of the $6p_z$ bands can be avoided for certain island heights. The $6p_z$ bands of the QWS formed in the magic height islands, whose electronic structure is depicted, do not even come within a binding energy of several kT of the Fermi level. The QWS from the 8 ML high islands is only faintly visible, but remains below E_F. The QWS formed for the intermediate coverages all have $6p_z$ bands that cross the Fermi level, and are therefore suppressed.

For Pb on Cu(111) I argued that the system stabilises into layers for which the QWS is furthest away from the Fermi level at $k_{||} = 0$. This is, however, only part of the full picture. The energy minimization does not only occur at $k_{||} = 0$, but, considering the lack of dispersion in the direction perpendicular to the surface, over the full range of $\boldsymbol{k}$ in all three dimensions. The fact that for In/Si(100) the formation of an 8 ML thick film is avoided (see Figure 3.17), and instead 7 and 9 ML thick layers are formed, is also an example of this principle. Although the $5p_z$ bands will cross the Fermi level for all three coverages, the 8 ML film is suppressed because for a larger $\boldsymbol{k}$ range the QWS will be close to E_F.

Considering the magic heights for Pb/C and the energy variations shown in Figure 3.34, the question arises why the 2 and 4 ML thick islands have not been previously observed for thin Pb layers. Over the full range of $\boldsymbol{k}$, their bands are further below the Fermi level than those of the 6 ML QWS, which is observed to be exceptionally stable on the √3 reconstruction of Si(111). Also the energy minima in Figure 3.34 are much deeper at 2 and 4 ML than at a thickness of 6 ML. A possible reason is that for Si(111) the charge transfer across the interface is larger than for vacuum or graphite, or in other words the phase shift at the interface will be larger. This will increase the value of φ_0 in Equation 3.1, and the whole damped sinusoidal function will slightly move to lower coverages. The points on this curve for 2 and 4 ML already have a high positive slope, and the surface energy may increase dramatically. On the other hand, at 6 ML the sinusoidal function has a negative slope, and a slightly larger phase shift will lower the surface energy. The second explanation is based on the fact that Pb and Si have a 6 % lattice mismatch and that, unlike for Pb on graphite, the Pb overlayer will try to adapt its lattice to that of Si(111). This induces a large amount of strain in the Pb layers. This strain is larger for thinner films, therefore increasing the surface energy of the 2 and 4 ML high islands, but hardly affecting the thicker films.

The deposition of aluminium on graphite does not directly lead to the formation of preferred heights. This is obvious from the as-deposited spectrum in Figure 3.25, where almost no features can be observed. After annealing the layer, islands with a height of 17, 18 and 19 ML are formed. Why islands of exactly these heights are formed can be explained by considering the theoretically expected QWS energies depicted in Figure 3.28. At a coverage of 20 ML, the next branch of QWS crosses the Fermi level, therefore causing a sudden increase in the total energy of the layer. The observed island heights form a local minimum in the layer energy, and can therefore be considered to be stable for this annealing temperature. When annealing at higher temperatures, the aluminium atoms have enough thermal energy to overcome the energy barrier for forming the 20 ML thick islands. At this temperature, the 20 and 21 ML islands can be formed, and coexist with the 17-19 ML high islands. After further annealing, the spectral weight actually shifts toward the Fermi level with the formation of a QWS right at E_F. At this temperature, the thermal energy of the atoms seems to be high enough to overcome all the energy barriers imposed by the variations of the total energy due to quantum size effects. The influence of QWS energies on the total surface energy seems to diminish, and classical effects take over. Within the classical picture, the surface energy of a film can be minimized by breaking it up into islands with a height comparable to its radius. In practice this means that constantly higher islands will be formed, especially on a substrate with a very low surface energy, as is the case for graphite.

Although both Al and Pb are simple s-p-metals, the response to quantum size effects and the formation of preferred or magic height islands is quite different for lead and aluminium. As for most other material properties, this can be explained in general terms by taking a detailed look at the electronic structure. For the formation of preferred heights, the interplay between the interlayer spacing and the electron wavelength at the Fermi level is the deciding factor. For lead, every monolayer can contain approximately three quarters of the Fermi wavevector ($d_{Pb} = {}^3/_4\ \lambda_{Pb}$), whereas for aluminium the ratio is two thirds ($d_{Al} = {}^2/_3\ \lambda_{Al}$). This means that for Pb, for every other layer the mismatch between the film thickness and the possible standing electron wave will either be zero or maximum. For Al the mismatch will only become zero at every third layer, and has a an intermediate value for the two layers in between. In the electronic growth theory, it is not the absolute value of the layer energy that is relevant, but its second derivative with respect to coverage. Because for Pb the oscillatory period of the mismatch between layer thickness and electron wavevector is shorter than for Al, the curvature of the total energy versus coverage will be larger. Therefore for Pb the stable heights are more preferred and the unstable heights are more strongly avoided. In a very convincing confirmation of these ideas, a recent STM experiment found that, for low coverages, aluminium avoids this long oscillation period by forming a 1.5 ML high island[25]. These islands consist of a normal 1x1 layer and a diluted $\sqrt{3}$x$\sqrt{3}$ layer, in total this creates an island height of 3.5 Å, which exactly corresponds to the electron wavelength in Al.

25 Y. Jiang, K. Wu, Z. Tang, Ph. Ebert, and E. G. Wang, to be published.

In conclusion, it has been shown that the formation of quantum well states can have a profound effect on the stability of the respective layers. Certain layer thicknesses are highly preferred, whereas others are avoided. The main driving mechanism is that, due to the changing binding energies of the QWS as a function of coverage, the total energy of the layer oscillates. The period of this oscillation can again influence the formation of stable and unstable heights, whereby a shorter period will create larger differences between preferred and avoided thicknesses. As a general rule of thumb, however, it can be stated that coverages that have their highest occupied QWS further away from the Fermi level ar more stable than those with a density of states close to E_F.